



Universiteit
Leiden
The Netherlands

The endothelial compartment as a disease modifier in bleeding disorders

Laan, S.N.J.

Citation

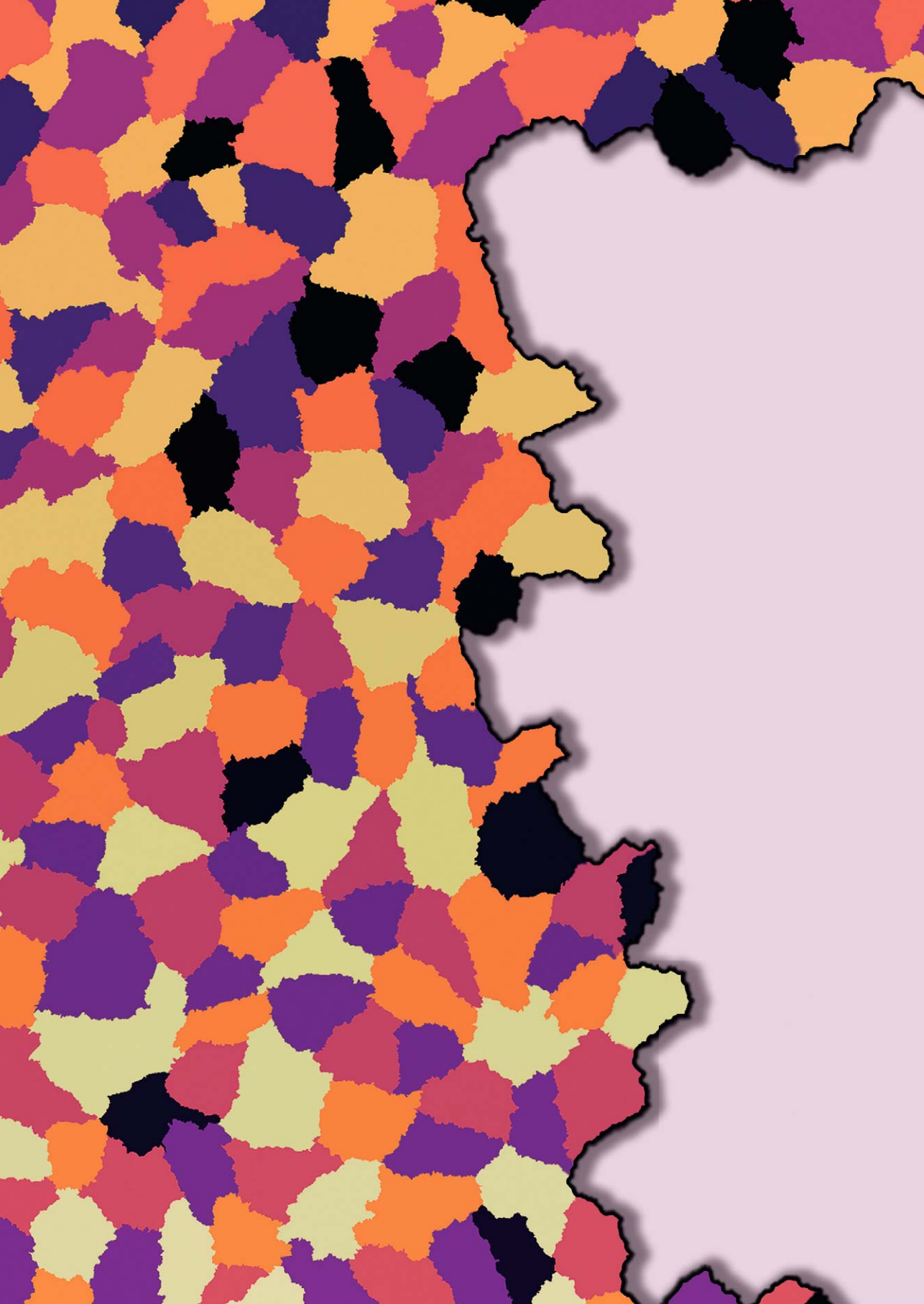
Laan, S. N. J. (2025, September 24). *The endothelial compartment as a disease modifier in bleeding disorders*. Retrieved from <https://hdl.handle.net/1887/4262075>

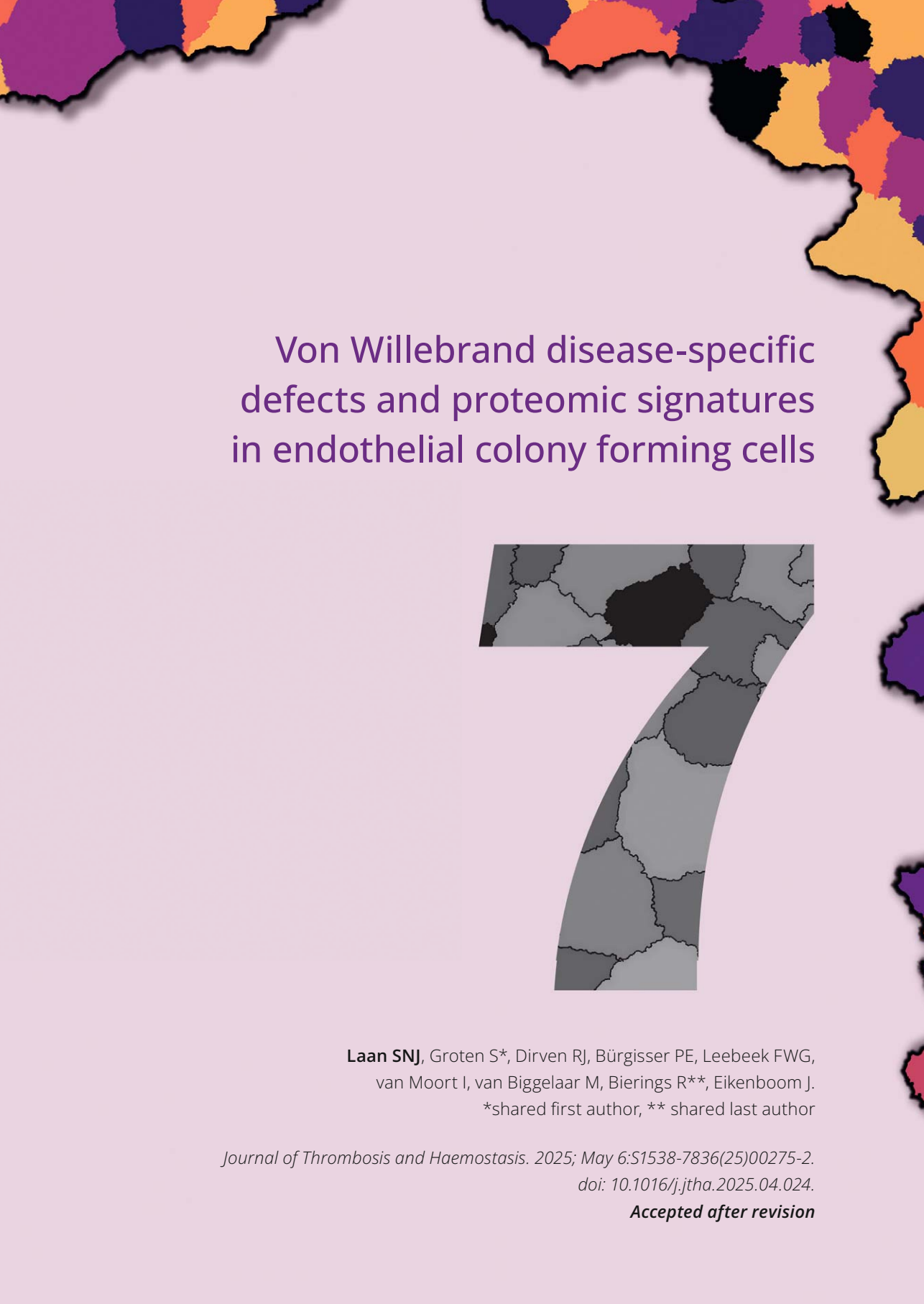
Version: Publisher's Version

License: [Licence agreement concerning inclusion of doctoral thesis in the Institutional Repository of the University of Leiden](#)

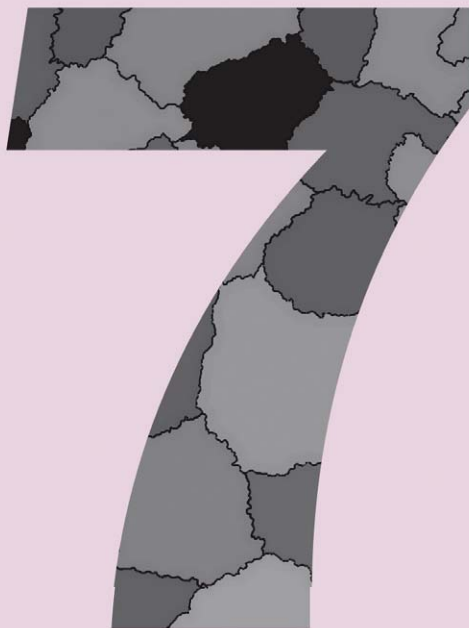
Downloaded from: <https://hdl.handle.net/1887/4262075>

Note: To cite this publication please use the final published version (if applicable).





Von Willebrand disease-specific defects and proteomic signatures in endothelial colony forming cells



Laan SNJ, Groten S*, Dirven RJ, Bürgisser PE, Leebeek FWG,
van Moort I, van Biggelaar M, Bierings R**, Eikenboom J.

*shared first author, ** shared last author

Journal of Thrombosis and Haemostasis. 2025; May 6:S1538-7836(25)00275-2.
doi: 10.1016/j.jtha.2025.04.024.

Accepted after revision

Abstract

Endothelial cells are crucial for hemostasis as they produce Von Willebrand factor (VWF). Von Willebrand disease (VWD) results from a deficiency of, or defects in, VWF. Here, we analyze the endothelial compartment of VWD patients with an unexplained decrease in VWF level or non-response to DDAVP using endothelial colony forming cells (ECFCs).

13 healthy controls and 10 VWD type 1 and 2 patients were included and a total of 29 ECFC clones were derived. Plasma was analyzed and ECFCs were morphologically and functionally characterized by qPCR, ELISA, imaging, migration assay and mass spectrometry.

VWF plasma levels were reduced in all patients. ECFCs were categorized into 2 previously defined transcriptional clusters and matched between patients and controls. Three ECFC clones, all from DDAVP non-responders, retained VWF in the endoplasmic reticulum (ER). Cluster 1 ECFCs from DDAVP non-responders had slower closing speeds in the migration assay and secreted more VWF antigen in rest than control ECFCs. Proteomic data of ECFC lysates showed overlap in clustering with RNA profiles, including ALDH1A1, TGFB1 and other EndoMT/ inflammatory markers. However, no patient group specific phenotype was observed. Finally, regulated secretion of VWF and Weibel-Palade body count in ECFCs were correlated with various secretory machinery components.

Lower plasma VWF was linked to reduced production and secretion by patient-derived ECFCs. Furthermore, non-response to DDAVP in some patients was explained by retention of VWF in the ER. The correlation between functional aspects of ECFCs and their qPCR and proteome profile yielded potential targets for further research.

Introduction

Endothelial cells play a key role in hemostasis. Von Willebrand factor (VWF) is one of the main components of primary hemostasis and is produced by endothelial cells and megakaryocytes. VWF is a large multimeric glycoprotein that binds to collagen and platelets, thereby initiating platelet plug formation upon vessel damage. VWF also binds to factor VIII and protects it from degradation. The protein is stored in specialized cigar-shaped secretory organelles called Weibel-Palade bodies (WPBs) (1, 2). These organelles can secrete their content continuously into the vessel which provides a steady level of VWF. However, endothelial cells can also be stimulated by injury or stress to rapidly secrete their content to increase circulating VWF levels (3).

When VWF is deficient or qualitatively defect, bleeding can occur, known as Von Willebrand disease (VWD) (4). This is the most common inherited bleeding disorder in humans found in ~1 in 100 individuals (5). The disease can be divided into 3 subtypes. Type 1 is hallmarked by low levels of functionally normal VWF, whereas in type 3, VWF is not present at all, making it the most severe type. Type 2 VWD is associated with qualitative defects in VWF, like impaired multimerization (type 2A), enhanced or spontaneous binding to platelets (type 2B), decreased binding to platelets or collagen (type 2M) or decreased binding to Factor VIII (FVIII) (type 2N) (4). VWD is usually treated by either administration of 1-deamino-8-D-arginine vasopressin (DDAVP), or by VWF concentrates (6). However, large inter individual differences in response to DDAVP are observed. Several studies have reported differences in response due to disease subtype, mutation, age or blood group (7-20), but the cause of the variation is not fully understood. Although, VWD is the most common bleeding disorder, it is difficult to diagnose due to the large heterogeneity and number of mutations or deletions in the *VWF* gene observed within patients (21). Adding to the complexity, roughly 30-50% of VWD type 1 patients do not have *VWF* gene variants and have been shown to present with a distinctly different bleeding phenotype (22-24). Current assays and genetic testing often do not explain the cause of bleeding in these patients and it is hypothesized that other modifiers cause the low levels and associated bleeding (25).

As endothelial cells are vital in the synthesis, storage and secretion of VWF, we hypothesize that they may play a role in the unexplained VWD phenotype of patients without *VWF* variant and may yield insight into the cause of the poor response to DDAVP. One way to study the molecular and pathophysiological aspects of patient endothelial cells is the endothelial colony forming cell (ECFC) model. One significant benefit of this model is its capability to generate clonally proliferative cells which exhibit endothelial traits, including the production and storage of VWF within WPBs, response to stimuli

and characteristic endothelial cobblestone-like morphology (26). When derived from patients, these cells can be used to study the pathophysiological mechanisms of VWD in the patients (27-31).

In this study, we aimed to investigate the endothelial compartment in the context of VWD as the endothelial cells may play a role in the unexplained low levels of VWF or poor DDAVP response in some patients. We found distinct retention of VWF in the endoplasmic reticulum (ER) in the ECFCs of some patients that did not respond to DDAVP. Furthermore, we highlight the inverse correlation between secreted VWF antigen (VWF:Ag) by ECFCs after stimulation and WPB count with cell area and the correlation between VWF levels and exocytotic machinery.

Materials & Methods

Patient inclusion and ethical approval

Patients were selected from the previous nationwide cross-sectional Willebrand in the Netherlands (WiN) study (32). Informed consent was obtained from 10 patients and 13 healthy donors. Healthy donors had not been diagnosed with VWD or any other bleeding disorder. Inclusion criteria for the patients were as follows: diagnosed with VWD and either 1) no known *VWF* variants or 2) with a *VWF* variant, but non-responsive to DDAVP. Complete response was defined as 2 times increase in VWF platelet binding activity (VWF:Act) from baseline at 1 hour after DDAVP and VWF:Act ≥ 50 IU/dL until 4 hours after DDAVP (32). At the moment of inclusion, the International Society on Thrombosis and Haemostasis Bleeding Assessment Tool (ISTH-BAT) (33) was obtained and blood samples were drawn (10 mL citrated and 50 mL heparinized blood).

Plasma coagulation factor levels

Citrated plasma samples from patients and controls at the time of inclusion were centrally measured for VWF:Ag, VWF:Act, VWF collagen binding (VWF:CB) and FVIII coagulant activity (FVIII:C). The assays that were used for these central measurements are described in the Supplementary Methods section. Furthermore, from the WiN database, historically lowest plasma levels and levels at the time of inclusion in the WiN study were also used in this study (32). Note that historical VWF activity was measured with different platelet binding assays. In this article all VWF activity levels will be indicated as VWF:Act.

Endothelial Colony Forming Cells acquisition

ECFCs were obtained following study protocols which were approved by the Leiden University Medical Center (LUMC and Erasmus MC (EMC) ethics review boards. Isolation and cell culture of ECFCs was performed as described previously (34). In short, isolation and culture procedures involved venipuncture to collect whole blood, isolation of PBMCs, and subsequent culture in EGM-18 medium (EBM-2 Basal Medium with EGM-2 supplements & growth factors (Lonza, or PromoCell) with 18% heat inactivated FBS (Thermo Fisher). At the EMC, not heat inactivated FBS was used. Clones typically emerged between days 10 and 21, and upon reaching confluency in three T75 flasks (at LUMC) or in four T75 flasks (at EMC) at passage 3, were frozen. A total of 29 clones were isolated in this study, with experiments conducted on clones at passage 5. Detailed information regarding each clone is provided in Table 1.

Brightfield and immunofluorescence image acquisition

For brightfield imaging, ECFCs at passage 5 were imaged three days after confluency was reached with the Leica MC170 HD camera attachment to the DMIL LED (2.5 and 5x lens) (Leica). For immunofluorescence imaging, staining and imaging were performed as described before (35). All samples were stained with antibodies against VWF, V-cadherin and nuclei were stained with Hoechst diluted in blocking buffer. In addition, ER was visualized by staining with antibodies against Protein Disulfide Isomerase (PDI). See Supplemental Table 1 for details on antibodies. Imaging for large tile scans was performed similarly as described before (35) although a 5x5 tile scan was made for a total area of 1059.84 x 1059.84 μm (23261 μm^2). For super resolution imaging, cells were imaged using the Zeiss LSM900 Airyscan2 upright confocal microscope with an 63x oil immersion objective.

Migration assay and image acquisition

For the cell migration assay, all samples were cultured in 48-well plates at passage 5. The protocol was followed as described previously (35). Briefly, each clone was randomly plated in six wells of a 48-well plate. Three days after confluency was reached, cells were labeled with CellTracker Green (Life technologies) diluted 1:10,000 in EGM-18 for 45 minutes. Three wells per clone were treated with 12.5 $\mu\text{g}/\text{mL}$ Mitomycin C (Sigma-Aldrich) for 2 hours while the remaining three wells received medium only. The confluent cell layer was damaged by making a scratch using a p100 pipet tip, after which the cells were imaged using the AF6000 (Leica) microscope with a 10x lens at 37°C and 5% CO₂. Each well was imaged every 30 minutes for 24 hours for visualization of cell migration. Time points 1, 2 and 3 had to be removed from analysis due to shifting of the plate during image acquisition.

Automated quantification of ECFC morphology and migration

Automated quantification of ECFC-parameters was done mostly with CellProfiler (version 4.2.1) (36). Confocal imaging tiles of ECFCs were analyzed using the purpose-made OrganelleProfiler pipeline as described previously (37). The pipeline was optimized as needed for the antibodies used and the measured intensity. For the current study we adjusted the OrganelleProfiler pipeline so that artefacts with high intensity, usually 6 to 7 times higher than the VWF signal, were identified and masked out of the image prior to WPB analysis. For the migration assay analysis, a previously developed CellProfiler pipeline was used to identify, count and track individual cells (35). Analysis parameters and pipeline modifications specific for this study are detailed in the Supplementary Methods section. The CellProfiler pipelines used for morphology and migration analysis are supplied in the Supplemental Files (file 1 and 2) and are made available on GitHub (<https://github.com/Clotterdam>).

Basal and stimulated release of VWF

Basal and constitutive release of VWF in EGM-18 medium by ECFCs was determined over 24 hours before the cells were stimulated as described previously (34). In addition to histamine, ECFCs were also exposed to 10 μ M Epinephrine (Sigma-Aldrich) with 100 μ M IBMX (Sigma-Aldrich) to trigger cAMP-mediated secretion of VWF. Cell lysates were collected and media and lysates were measured by VWF:Ag enzyme-linked immunosorbent assay (ELISA) as was described previously (38).

Mass spectrometry sample preparation and acquisition and analysis

For mass spectrometry analysis of EC proteomes, samples were digested with trypsin as described previously (39). Tryptic digests were transferred to an Evotip Pure (Evosep) according to manufacturer's guidelines and analysed with an Evosep One liquid chromatography (LC) system (Evosep) coupled to a TimsTOF HT mass spectrometer (Bruker). Peptides were separated on a 15 cm \times 150 μ m, 1.5 μ m Performance Column (EV1137 from EvoSep) with the 30 samples per day gradient. Buffer A was composed of 0.1 % formic acid, buffer B of 0.1 % formic acid in acetonitrile (Biosolve, NLD). Peptides were ionized and electro sprayed into the mass spectrometer. Data was acquired in DIA-PASEF mode, using an MS1 scan range of 100 - 1700 m/z. Accumulation time was set at 100 ms with a duty cycle of 100%. MS2 acquisition was performed using 32 pyDIAID (40) optimized mass and ion mobility windows, ranging from 400.2 - 1500.8 m/z and 0.70 - 1.50 1/k0 with a cycle time of 1.80 s. A collision energy of 20.00 eV at 0.6 1/k0 and 59 eV at 1.60 1/k0 was used. Raw mass spectrometry data files were processed using the DIANN software (version 1.8) as previously reported (39). Data was analyzed using R 4.2.3 / Rstudio (2022.07.02). Sample S34 could not be included in the analysis due to technical reasons. Detected proteins were filtered for proteotypic and at least

one unique peptide per protein. Proteins should be quantified in at least six different samples. Label free quantification (LFQ) values were transformed in \log_2 scale. Missing values were imputed by normal distribution (width = 0.3, shift = 1.5), assuming these proteins were close to the detection limit. All LFQ values are available in Supplemental File 3.

RNA isolation and quantification with quantitative PCR (qPCR)

All ECFC clones were cultured in 24-well plates at passage 4 and were kept in culture for 5-7 days after they reached confluency. Isolation of RNA, synthesis of cDNA and subsequent characterization of ECFCs into clusters by a qPCR gene panel were performed as described previously (35). Primer sequences of all genes tested are available in Supplemental Table 2. Measurements were analyzed using the comparative Ct method where GAPDH was used as the housekeeping gene. Results from the qPCR were analyzed using the prcomp function from stats in Rstudio (version 3.6.2). The script is supplied as Supplemental File 4 (also made available on GitHub (<https://github.com/Clotterdam>)).

Statistical Analysis

Functional aspects of ECFCs between controls and patient groups were compared by Mann-Whitney U test (not normally distributed) and unpaired T test with Welch's correction (normally distributed). Kruskal-Wallis one way ANOVA was used when comparing more than 2 groups. Plasma measurements are presented as boxplot with median or as points per ECFC clone with mean for all others. P value < 0.05 was considered statistically significant. Data were analyzed using GraphPad Prism 9.3.1 (GraphPad Software, San Diego, CA, USA) unless otherwise indicated. For proteome analysis, partition around medoids (PAM)-based clustering was performed using the Cluster package (41), employing a Kmax of 20 with 100 iterations each. To determine differentially abundant proteins, moderated t-tests were performed using LIMMA (42, 43). A BH adjusted $p < 0.05$ and \log_2 fold change > 1 was considered significant and relevant. Spearman correlations were calculated using Hmisc (44). Gene ontology term enrichment was performed using the clusterProfiler package (45), enrichments with a BH adjusted p-value < 0.05 were considered significant.

Results

VWD study population and ECFC isolation

In this study, we aimed to investigate the endothelial compartment as a potential modifier of VWD phenotype by studying ECFCs derived from 13 healthy controls and

from two groups of VWD patients in which an endothelial contribution to their disease etiology is plausible: (1) patients without pathogenic *VWF* gene variants with a normal response to DDAVP and (2) patients with VWD with a known pathogenic mutation in *VWF* who do not respond to DDAVP (Figure 1A). Patients were classified as type 1 (6 patients) or type 2 (4 patients) VWD based on the current VWD diagnostic guideline (46). Detailed characteristics of the patients and controls are shown in Table 1. Plasma coagulation factor levels (VWF:Act, VWF:Ag, VWF:CB and FVIII:C) were determined again at time of inclusion in this study (Figure 1B-E). All measured coagulation factors were significantly lower in DDAVP non-responders when compared to healthy controls. VWF and FVIII levels were also reduced in VWD patients without pathogenic *VWF* variants, but this was only statistically significant for VWF:CB. When compared to historically lowest levels until WiN inclusion and levels measured during the WiN inclusion (12-16 years ago) (32), current levels have partially corrected (Figure 1B-E) which is likely due to age-dependent increase in plasma VWF levels (23, 47-49).

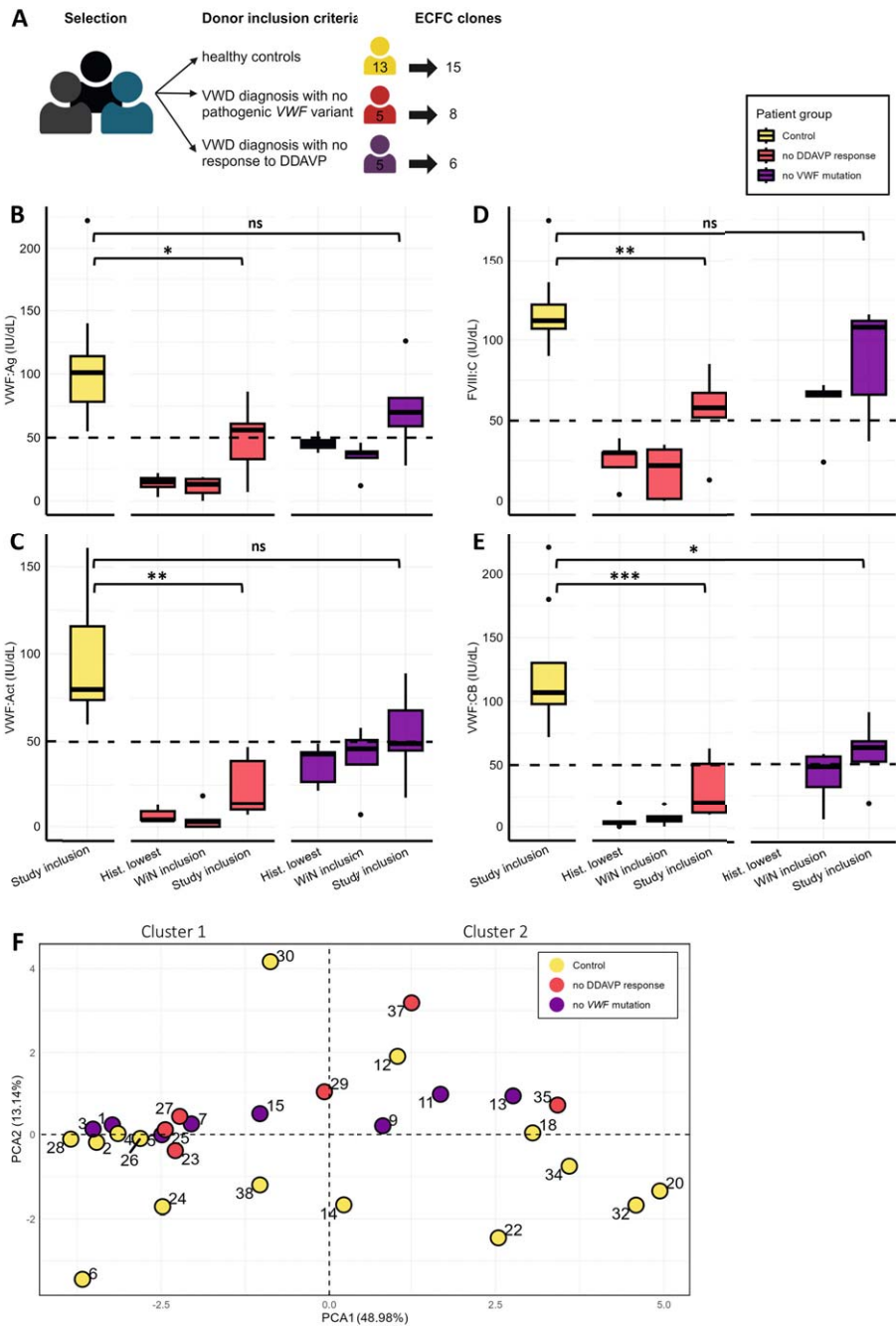


Figure 1. Patient and control plasma levels and ECFC characteristics. A) Schematic overview of donor inclusion. Boxplots of B) VWF:Ag, C) VWF:Act, D) FVIII:C and E) VWF:CB in the plasma of VWD patients and controls at inclusion in the current study. Furthermore, historically lowest factor

levels and levels at time of inclusion in the WiN (32) are shown. Statistical analysis by Kruskal-Wallis one way ANOVA, * $p < 0.05$, ** $p < 0.01$. values 1.5 times outside the interquartile range (IQR) are shown as black dots. Note that previously, VWF activity was measured with different platelet binding assays. In this article all VWF activity levels will be indicated as VWF:Act. F) PCA plot showing heterogeneity between ECFC clones. All clones on the left of the y-axis were categorized as cluster 1, and clones on the right as cluster 2. Numbers correlate with sample numbers and color indicates which group the clone belongs to, controls (yellow), VWD patients without DDAVP response (red) and VWD patients without VWF variant (purple). Abbreviations: PCA = Principal Component Analysis; Hist. = Historically; VWF = von Willebrand factor; Ag = Antigen; Act = Activity; WiN = Willebrand in the Netherlands; CB = Collagen binding; DDAVP = 1-deamino-8-D-arginine vasopressin.

ECFC isolation and RNA based characterization

To study VWD-specific signatures of endothelial cells, we isolated at least 1 ECFC clone from all patients and controls. When multiple clones were isolated per donor 2 were taken along in this study, which resulted in 15 clones from controls and 14 from patients (Figure 1A). A complete overview of the ECFC clone and donor characteristics is shown in Table 1. All clones displayed characteristic cobblestone-like endothelial morphology although with large heterogeneity (Supplemental Figure 1) It is widely recognized that substantial phenotypic heterogeneity can exist between ECFC clones isolated from healthy controls and even from the same individuals (34, 38), which can be explained by the existence of at least two discrete transcriptional clusters of ECFCs (35). We carried out a qPCR-based transcriptional analysis of ECFC clones as described previously (35) (Supplemental Table 2) that can distinguish between the aforementioned phenotypic clusters of ECFCs. To visualize the variation between clones we performed principal component analysis (PCA) (Figure 1F), which revealed large intra- and inter-individual heterogeneity and allowed us to categorize ECFC clones in cluster 1 and cluster 2 ECFCs (Table 1). To ensure correct comparison between control and patient ECFCs, we will use this categorization in all following assays to compare ECFC clones with clones within their assigned cluster.

Morphological and migratory characterization of VWD patient-derived ECFCs

Morphology of ECFCs was studied to investigate whether defects in the secretory pathway or abnormal distribution, count and/or shape of WPBs contribute to the VWD phenotype of the patients. All ECFCs were imaged for VWF, VE-cadherin and their nuclei (Figure 2A). Clone S38 is shown as a representative for the control ECFCs and shows typical cigar-shaped WPBs. We observed that 3 out of 5 ECFCs from patients with DDAVP non-response showed signs of retention of VWF in the ER (S29 shown as representative clone of other ECFCs S25, S27 and S35), which was confirmed by PDI staining (Supplemental Figure 2). No uniform morphological phenotype was seen in patients without pathogenic VWF variants, but S11 did display very large cells and small

and round WPBs. ECFC characteristics were quantified using an automated image-analysis pipeline developed in CellProfiler (37). Great variation in cell count, WPB count per cell, organelle eccentricity and relative distance to the nucleus between all ECFCs was observed (Figure 2B-E) as was also shown previously in healthy controls (35, 37). Between patient groups and controls, only mean organelle eccentricity was found to be significantly lower in cluster 1 ECFCs of patients without DDAVP response. This effect was primarily attributable to the ECFCs that showed ER retention, which on average had lower organelle eccentricity (0.637 ± 0.015 vs. control 0.721 ± 0.039) and WPB count per cell (35.97 ± 24.20 vs. control 132.30 ± 27.60). Together this data highlights a distinct phenotype in ECFCs of DDAVP non-responders that results in retention of VWF in the ER, thereby reducing its availability for stimulus-induced release of VWF from WPBs.

Table 1. Patient and control ECFC characteristics.

ID	Diagnosis	DNA Change	Protein Change	Age at inclusion	sexe	Blood group	ISTH-BAT bleeding score	Hist. lowest			Day of detection**	Time in culture***	Cluster
								VWF:Ag (U/dL)	VWF:Act (U/dL)	sample#			
1	Control	n.d.	n.a.	22	Female	O	0	n.d.	n.d.	S2	13	10	1
2	Control	n.d.	n.a.	28	Female	n.d.	n.d.	n.d.	n.d.	S4	13	11	1
3	Control	n.d.	n.a.	29	Female	O	4	n.d.	n.d.	S6	19	30	1
4	Control	n.d.	n.a.	23	Female	n.d.	n.d.	n.d.	n.d.	S12	21	38	2
5	Control	n.d.	n.a.	27	Female	O	0	n.d.	n.d.	S14	13	23	2
6	Control	n.d.	n.a.	28	Male	n.d.	n.d.	n.d.	n.d.	S20	15	27	2
7	Control	n.d.	n.a.	30	Female	B	1	n.d.	n.d.	S18	14	44	2
8	Control	n.d.	n.a.	27	Male	n.d.	n.d.	n.d.	n.d.	S22	14	26	2
9	Control	n.d.	n.a.	25	Female	AB	1	n.d.	n.d.	S24	13	29	1
10	Control	n.d.	n.a.	23	Female	B	n.d.	n.d.	n.d.	S26	14	23	1
11	Control	n.d.	n.a.	29	Male	n.d.	n.d.	n.d.	n.d.	S28	10	14	1
12	Control	n.d.	n.a.	23	Male	n.d.	n.d.	n.d.	n.d.	S30	11	17	1
13	Control	n.d.	n.a.	64	Male	n.d.	n.d.	n.d.	n.d.	S32	21	54	2
14	Control	n.d.	n.a.	32	Male	n.d.	n.d.	n.d.	n.d.	S34	16	53	2
15	Control	n.d.	n.a.	32	Male	n.d.	n.d.	n.d.	n.d.	S38	13	24	1
16	VWD Type 1	no	n.a.	32	Female	A	23	42	49	S1	8	13	1
17	VWD Type 1	no	n.a.	32	Female	A	23	42	49	S3	11	7	1

Table 1. Continued.

ID	Diagnosis	DNA Change	Protein Change	Age at inclusion	sexe	Blood group	ISTH-BAT bleeding score	Hist. lowest			Day of detection**	Time in culture***	Cluster
								VWF:Ag (U/dL)	VWF:Act (U/dL)	sample#			
15	VWD Type 1	no	n.a.	66	Female	O	14	38	27	S5 S7	13 15	19 20	1 1
16	VWD Type 1	no	n.a.	39	Female	O	9	48	44	S9	16	35	2
17	VWD Type 1	no	n.a.	50	Male	O	24	55	43	S13	17	45	2
18	VWD Type 2A	no	n.a.	66	Female	O	14	45	22	S11 S15	9 16	28 26	2 1
19*	VWD Type 2B	4022G>C	Arg1341Pro	73	Male	O	12	11	4	S23	17	20	1
20*	VWD Type 2A	2771G>A	Arg924Gln	88	Male	O	14	15	4	S25	19	25	1
21*	VWD Type 2A	4120C>T	Arg1374Cys	21	Male	n.d.	10	18	9	S29	14	32	1
22*	VWD Type 1	421G>A + 6937C>T	Asp141Asn + Arg2313Cys	39	Female	O	12	22	14	S27 S35	13 15	20 21	1 2
23*	VWD Type 1	3614G>A	Arg1205His	74	Female	B	12	3	4	S37	12	39	2

*Did not respond to DDAVP. **Number of days after inclusion. ***From day of detection to freezing (in days). Abbreviations: n.d. = not determined; n.a. = not applicable; ISTH-BAT = international society of thrombosis and hemostasis bleeding assesment tool; VWD = von Willebrand Disease; hist = historically; Ag = Antigen.

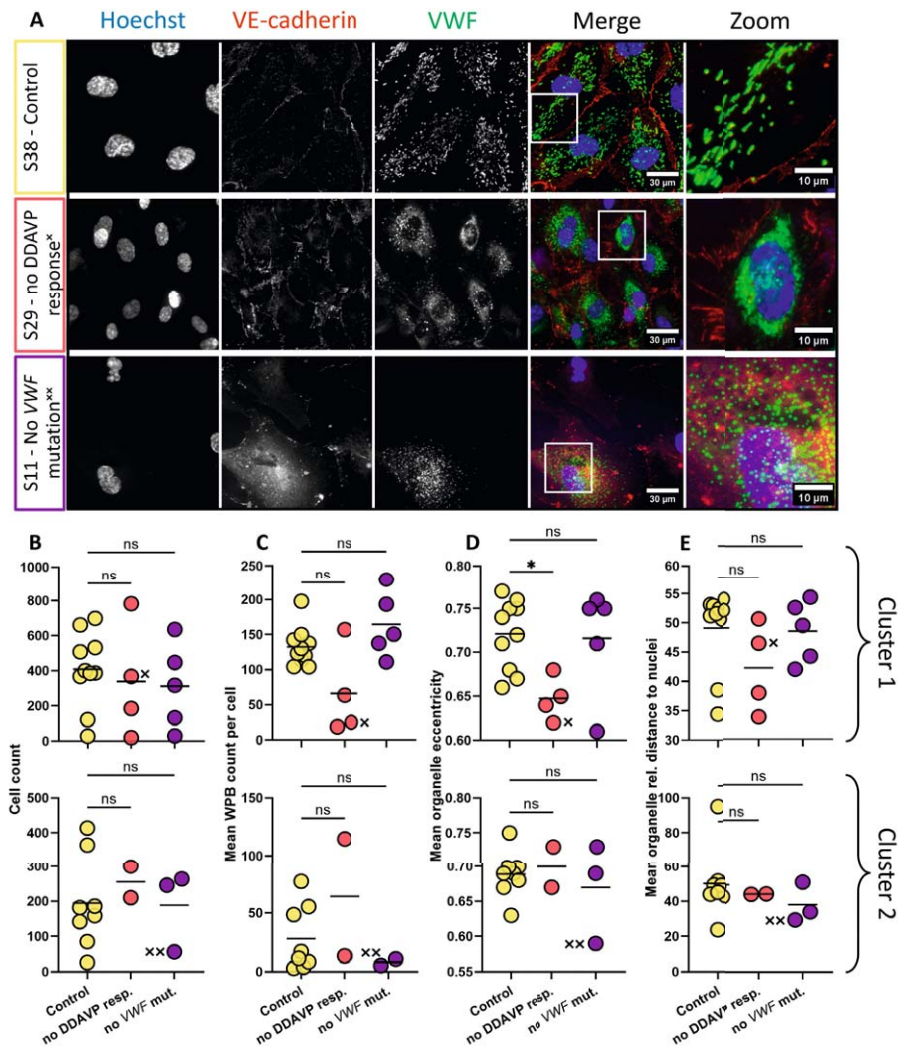


Figure 2. Morphological differences of VWD derived ECFCs. Phenotypic profiling of all ECFCs was done using tile scans (1123261 μ m²). ECFC clones were analyzed per cluster and stained with Hoechst (blue) and antibodies against VE-cadherin (red) and VWF (green). A) Representative confocal images of a control ECFC clone (top - S38), a patient with retention of VWF in the ER (middle - S29) and a patient ECFC with round WPBs (bottom - S11). Scale bar represents 30 μ m. The white box indicates the area that is enlarged by 3x of the merge (scale bar represents 10 μ m). Images were taken with a 63x objective. B) Cell count per surface area of the tile scan. C) Mean WPB count per cell per ECFC clone. D) Mean eccentricity of WPBs per ECFC clone. E) Distance of the WPB to the nucleus relative to their position in the cell in percentage. S29 and S11 values are indicated by x and xx respectively in B-E. Values per ECFC clone are shown and the line shows the mean. Kruskal-Wallis one way ANOVA was performed; * p < 0.05. Abbreviations: VWF = von Willebrand factor; DDAVP = 1-deamino-8-D-arginine vasopressin; ns = not significant; resp = responder; mut = mutation.

It has been shown that VWF plays a role in migration, proliferation and angiogenesis of endothelial cells (50) and that some type 1 and 2 VWD patient-derived ECFCs had lower directionality in wound healing assays (51). Therefore, we also analyzed the migration behavior of all ECFCs using a scratch wound migration assay (Supplemental Figure 3A). We observed that cluster 1 DDAVP non-responder ECFCs have a slower closing speed when compared to control ECFCs, while cluster 2 ECFCs from DDAVP non-responders close the scratch faster than controls (Supplemental Figure 3B). No significant differences were observed for speed of movement, X trajectory and linearity (Supplemental Figure 3C). However, samples 25, 27 and 29 in cluster 1 did show markedly decreased X trajectory. This suggests that ECs with observed ER retention and decreased VWF levels also have implicated migratory processes.

Impaired synthesis and secretion upon stimulation of patient ECFCs

We investigated whether production of VWF and secretory capabilities of the ECFCs may clarify the low VWF levels or lack of response to DDAVP. We measured basal VWF secretion over 24 hours (Figure 3A), intracellular VWF content in the lysate (Figure 3B) and regulated secretion of VWF following Ca^{2+} - (histamine) and cAMP-mediated (epinephrine) stimulation (Figure 3C-D). Cluster 1 control ECFCs secrete more VWF:Ag in rest than ECFCs from patients that did not respond to DDAVP. There is no difference between the ECFCs from controls and patients without VWF variant. Histamine and epinephrine stimulated release from ECFCs derived from patients without DDAVP response show a trend to lower response than controls. ECFCs derived from patients with no VWF mutation responded similarly to histamine and epinephrine stimulation as the control ECFCs. ECFC VWF synthesis and secretion was correlated to plasma VWF levels (Figure 3E-H). ECFCs in cluster 1 showed positive correlations between plasma VWF:Ag levels and all ELISA measurements while there was no correlation in cluster 2 ECFCs. This suggests that cluster 1 ECFCs are a good representative of VWF synthesis and secretion in the vessels of the patients.

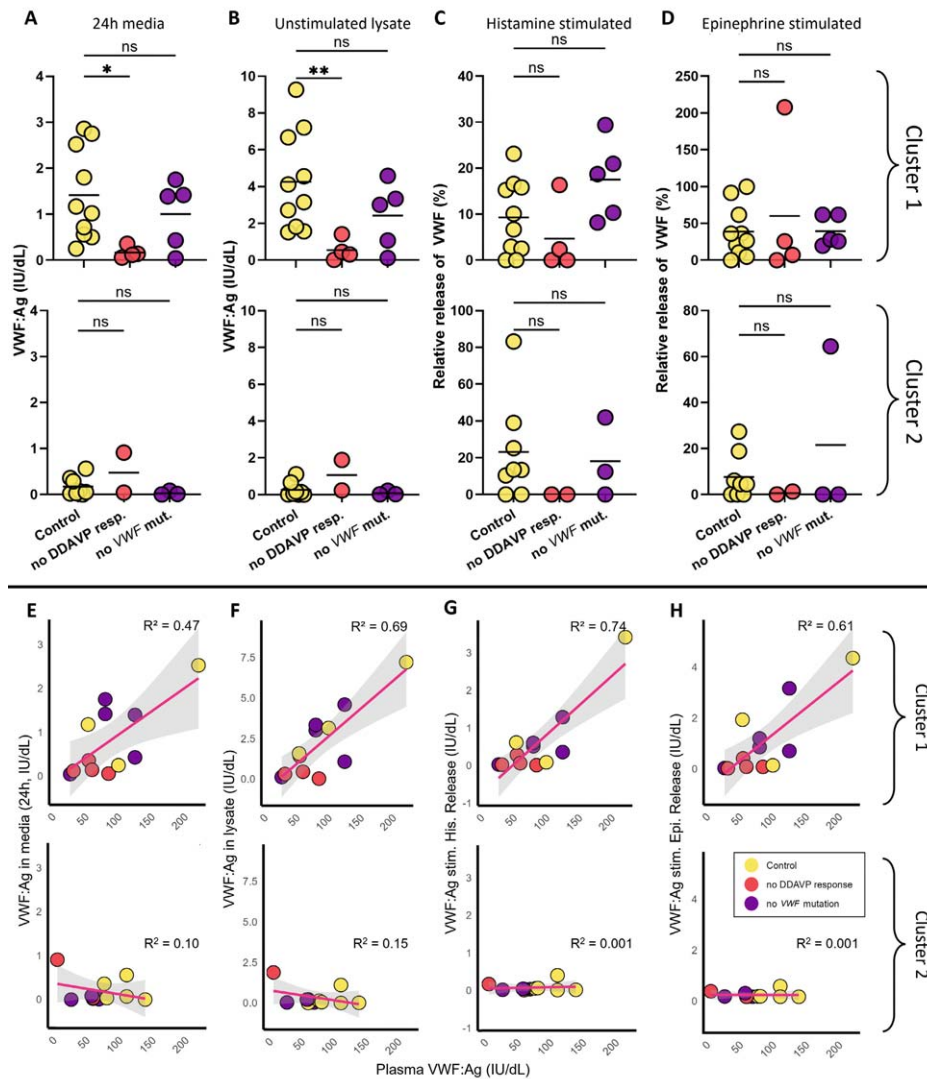


Figure 3. VWF production and secretion lower in patient ECFCs. ECFCs were grown in culture until confluent and then stimulated by histamine and epinephrine + IBMX to secrete VWF. VWF:Ag (IU/dL) levels as measured by ELISA are shown per ECFC clone. A) VWF levels secreted in media during 24 hours of culture of ECFCs preceding the stimulation. B) VWF levels in the lysates of unstimulated cells (DMSO exposure only) C) Secretion of VWF after 1 hour of stimulation as a percentage of the total amount of VWF in the cell. Calculated as the released VWF:Ag in media minus VWF:Ag released without stimulant (DMSO) divided by the total amount of VWF in the cell (the lysate of the unstimulated cells). If stimulated release was not higher than the negative control a value of 0 was noted. Plasma VWF:Ag measurements were correlated to the levels of VWF:Ag secreted by the ECFCs in rest (E), in the lysate (F), secreted after histamine stimulation (G) and secreted after epinephrine + IBMX stimulation (H). Statistical analysis by Kruskal-Wallis one way ANOVA, * $p < 0.05$, ** $p < 0.01$. R^2 was calculated by linear regression. Abbreviations:

DDAVP = 1-deamino-8-D-arginine vasopressin; VWF = von Willebrand factor; DMSO = Dimethyl sulfoxide; ns = not significant; his = histamine; epi = epinephrine.

VWD does not drive disease-specific proteomic differences

Next, we investigated whether we could find differences in protein abundance in ECFCs derived from VWD patients. Therefore, we performed unbiased proteomics on 28 ECFC clones using a bottom-up, label-free quantification mass spectrometry workflow (Figure 4A). On average, 8,349 proteins were quantified per sample (Supplemental Figure 4A) with an overall high correlation (Supplemental Figure 4B). Based on principal component analysis, we did not observe a clear distinction between controls and the 2 VWD patient categories (Figure 4B). PAM clustering of the proteomes, identified three ECFCs clusters (A,B,C) (Figure 4C) of which clusters A and B partially overlapped with the annotation based on the qPCR panel (Figure 4D). Statistical analysis comparing ECFCs derived from healthy controls with ECFCs derived from VWD patient groups showed no group-specific differences ($\text{LFC} > 1$, $p < 0.05$), irrespective of proteomics clustering (A,B,C) or subdivision in the qPCR panel (1,2) (Figure 4D-F). Comparison of individual patient ECFC clones versus controls within the proteomics clusters did reveal clone-specific alterations (Supplemental Figure 4C). However, the observed heterogeneity in ECFC clones derived from the same donor (Supplemental Figure 4D) combined with marginal overlap in regulated proteins between ECFCs clones from the same VWD donor (Supplemental Figure 4E), hampers interpretation of donor-specific differences. Taken together, this highlights the challenge to dissect VWD-specific defects in the individual patient.

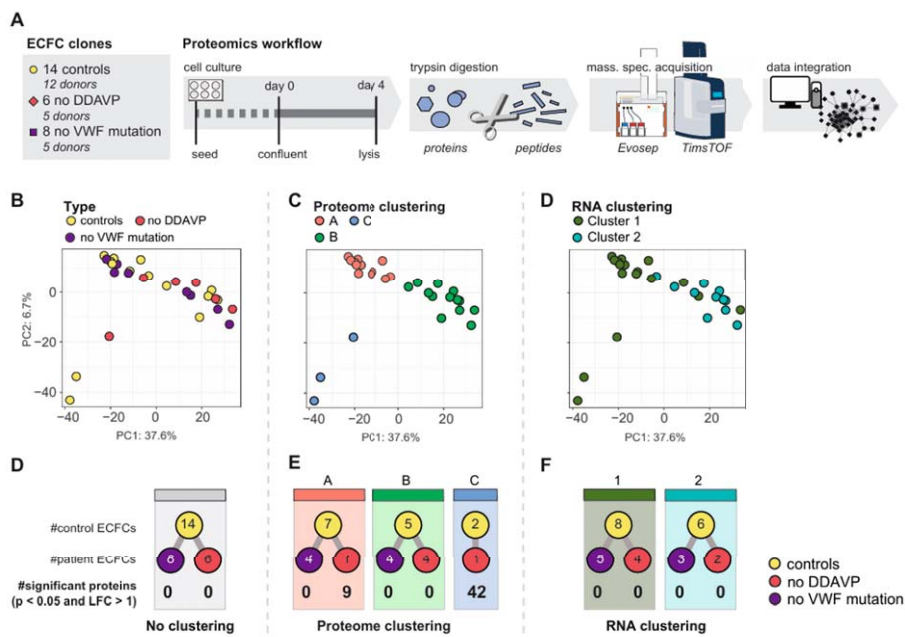


Figure 4. VWD does not drive disease-specific proteomic differences A) Schematic overview of proteomics workflow. Principal component analysis (PCA) of proteomes across PC1 and PC2, colored based on B) disease type, C) proteomics based clustering and D) qPCR based division. Overview of samples and significantly regulated proteins (t-test, $p < 0.05$ and $LFC > 1$) between D) disease type versus controls, E) disease type versus control per proteome cluster and F) disease type versus controls per qPCR based distinction. Abbreviations: DDAVP = 1-deamino-8-D-arginine vasopressin; VWF = von Willebrand factor; PC = principal component, LFC = Log fold change.

Proteomic signatures of heterogenous ECFC phenotypes

To further investigate endothelial heterogeneity in the context of VWD, we explored the differences that drive separation into clusters A,B,C (Figure 4C). On a morphological level, cluster A contained ECFCs with hallmark cobblestone morphology, while cluster B contained cells with a more inflamed and mesenchymal-like phenotype (Figure 5A), in agreement with qPCR segregation. Among the proteins driving the most variation between proteomic clusters A and B, were ALDH1A1, CLU, and VWF (increased abundance in cluster A) and TGFBI, CD44 and TAGLN (increased abundance in cluster B) which were previously described separating cobblestone-mesenchymal phenotypes by RNA-seq (34) (Figure 5B-C). In total, 316 of the 451 significantly different proteins between group A and B were identified in that study on transcript level as well (Supplemental Figure 5A-B). Interestingly, cells in cluster C showed a unique phenotype of spindle-like ECs that diverged from both other clusters. The variation across PC2, that mostly separated cluster C, was driven by RELN, TIMP3 and CEACAM1 among others

(Supplemental Figure 5C-D). In total 345 proteins were differentially abundant in cluster C compared to both other clusters ($LFC > 1$, $p < 0.05$) (Figure 5D). Cell-type-specific enrichment analysis of the upregulated proteins using WebCSEA (52) enriched highest for lymphatic ECs (Figure 5E). Moreover, lymphatic markers PROX1, VEGFR3 (FLT4) and, to a lesser extent, LYVE1 (53-55) were all more abundant in cluster C ECFCs (Figure 5F), suggesting these clones are of lymphatic endothelial lineage.

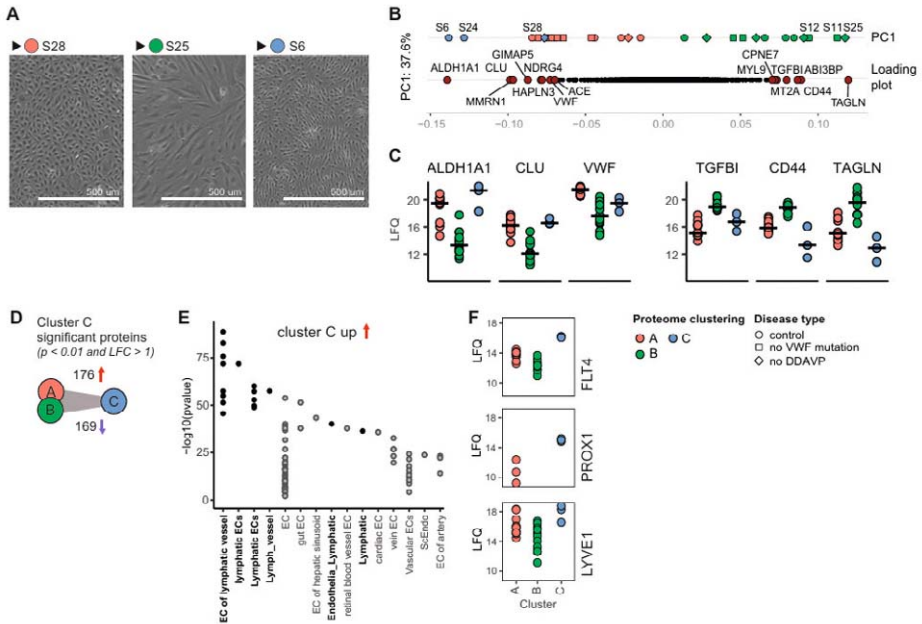


Figure 5. Proteomic signatures of heterogeneous ECFC phenotypes A) Brightfield images of hallmark ECFC clones per proteomic cluster, scale bar indicates 500 μm . B) Distribution of samples and loading plot across PC1, shape indicates disease type (control – circle, no DDAVP – diamond, no VWF mutation – square). Highest positive and negative separating proteins in the loading plot are highlighted in red and labeled. C) Dot plots of protein LFC values with high positive and negative separation across PC1. D) Number of up- and downregulated proteins (t-test, p -value < 0.05 , $LFC > 1$) in Cluster C versus both other clusters. E) Top 15 WebCSEA enriched endothelial cell subtype terms of upregulated proteins in group C. Colors indicate lymphatic EC terms (black) and other EC terms (grey). F) Dot plots of lymphatic proteins LFC values. PC = principal component, LFC = Log fold change, LFC = label-free quantification.

Combined data integration to decipher proteomics profiles in the context of VWF

To investigate proteomic profiles in the context of VWF across a heterogeneous ECFC population, we integrated VWF secretion, qPCR cluster profiles, morphological and functional data with protein expression profiles. Correlation analysis revealed

that abundance of an extensive network of proteins ($n = 2173$) was associated with a functional or cell biological outcome (spearman correlation coefficient > 0.7) (Supplemental Figure 6A). As expected, VWF:Ag levels in lysates and secreted VWF measured by ELISA correlated highly with the proteome VWF LFQ measurements (spearman correlation > 0.85) (Supplemental Figure 6B). VWF LFQ, VWF:Ag and secreted VWF levels also correlated positively with cell - and WPB count, and inversely with cell area (Supplemental Figure 6A). Proteins positively correlating with histamine-induced VWF secretion ($n=791$), enriched predominantly for the gene ontology biological process term "RNA processing" and proteins inversely correlated ($n=550$) enriched for "Endomembrane system" (Figure 6A). To specifically look for proteins associated with the VWF exocytosis machinery and WPB bodies, we highlighted known and putative WPB interactor proteins (2) and found that important adaptors in VWF release were positively correlated with increased VWF release, such as RAB27A, RAB3D, and SYTL4(56-58), while others such as GBF1 which is important in ER-Golgi trafficking of VWF was negatively correlating (Figure 6B). Of these proteins only RAB3D also positively correlated with WPB count per cell (Figure 6C). This suggests, while both RAB3D and RAB27A are important in WPB release, RAB3D also functions in managing WPBs in steady state. Surprisingly, IGFBP7, a protein known to be present in WPBs (59), is lower in abundance when more WPBs are present per cell (Figure 6D). Moreover, 18 mitochondrial proteins correlated positively with WPBs count of which mitochondrial membrane protein AGK had the highest correlation. Finally, correlating proteins to organelle eccentricity, which is a proxy for ER retention, were limited. However, several members of the vacuolar-ATPase (ATP6V-B1,-E1,-G1,-H1) negatively correlated with organelle eccentricity (Figure 6E). Counterintuitively, although the v-ATPase proton pump is required for the maturation of WPB bodies (59-61), our analysis shows that higher levels of this protein correlated with round WPB bodies (Figure 6F).

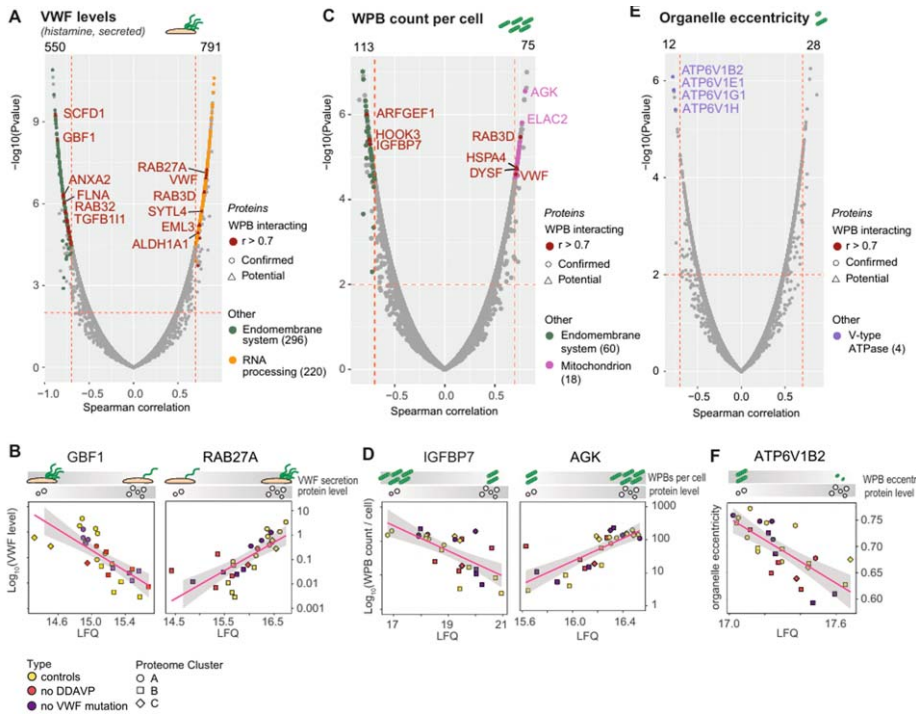


Figure 6. Proteomic and functional data integration A) Spearman correlation plot of histamine-induced secreted VWF levels with protein LFQ levels and B) protein correlations of interest. C) Spearman correlation plot of WPB count per cell with protein LFQ levels and D) protein correlations of interest. E) Spearman correlation plot of organelle eccentricity with protein LFQ levels and F) protein correlation of interest. For all Spearman correlation plots, correlation > 0.7 and p value < 0.01 are indicated by dotted red lines. Total number of proteins above cutoffs are indicated at the top of graph. WPB interacting proteins are indicated in red. Major enriched GO-terms per functional output and number of proteins per term are shown. Abbreviations: WPB = Weibel-Palade body; DDAVP = 1-deamino-8-D-arginine vasopressin; VWF = von Willebrand factor; DMSO = Dimethyl sulfoxide; his = histamine; epi = epinephrine, WPB = Weibel-Palade body, LFQ = label free quantification.

Discussion

ECFCs have been used to study biological processes in endothelial cells and to elucidate the pathogenic mechanisms of various diseases (29, 30, 51). There is a lot of variability in bleeding phenotype in patients with VWD (4) and it is hypothesized that other modifiers cause the low levels of VWF and associated bleeding (25) or perhaps non-response to DDAVP treatment. Therefore, in this study, we used ECFCs to attempt to unravel those mechanisms. Patients were previously diagnosed with VWD based on reduced

levels of plasma VWF:Ag and VWF:Act which correlated with low levels of produced and secreted VWF by ECFCs. Furthermore, we observed retention of VWF in the ER which was connected with very low levels of secreted VWF. Proteomic characterization of the ECFC clones yielded distinct clusters of ECFC clones that were not dependent on patient groups. Proteomic clustering overlapped with RNA based clustering and yielded a third cluster in this study, which seems to be of lymphatic endothelial lineage. Finally, comparing functional outcomes to proteomics, we observed that VWF levels and WPB count per cell correlated inversely with cell area and regulated secretion of VWF and Weibel-Palade body count in ECFCs were correlated with various secretory machinery components. Protein regulation showed strong enrichment of DNA and mRNA processing in cells with high VWF levels and a smaller cell area.

Despite the advantages of ECFCs, considerable phenotypic heterogeneity has been observed (34, 35, 38) which are influenced by day of initial appearance of ECFCs (34), passaging (62), and duration in culture (63, 64). Interestingly, the proteomic heterogeneity between clones was remarkably similar to the transcriptomic differences observed previously (35), even though different ECFCs, cultured in separate labs, were used. 316 from the 451 significantly different proteins between group A and B were measured by RNA-seq previously (35). This large overlap indicates that ECFCs maintain similar patterns on both protein and RNA expression level. Furthermore, endothelial to mesenchymal (EndoMT) associated proteins TGFBI, TGFB2 and BMP2 (65) were also found to be significantly different at the proteome level.

While the origin of circulating ECFCs is uncertain, the heterogeneity that we observed between clones resembles the differences in expression profiles between endothelial cells from distinct vascular beds (39, 66). The proteomic signature showed a distinct cluster enriched for ECs of lymphatic endothelial lineage. These cells were visually smaller and more spindle-like compared to other ECFC clones and they had higher protein levels of transcription factors PROX1 (67) and CEACAM1, which are important in the formation of new lymphatic vessels (68). Whether the observed ECFCs respond differently to external stimuli remains to be elucidated, but provides an interesting avenue to investigate vascular bed-related differences using ECFCs.

We hypothesized that unexplained non-response to DDAVP could be caused by modifiers outside of *VWF*. ECFCs that showed retention of VWF in the ER were all derived from DDAVP non-responsive patients that carried *VWF* mutations. The p.Arg924Gln mutation (S25) is associated with reduced VWF and FVIII levels (69), but ER retention in previous studies has not been confirmed through any staining. S27 and S35 (from the same patient) carry p.Asp141Asn and p.Arg2313Cys. The variant p.Asp141Asn has been

shown to cause ER retention in transfected HEK cells (70), which we now confirmed in ECFCs carrying this mutation. Finally, p.Arg1374Cys (S29) is still disputed as causing either VWD type 2A or 2M (71), but we show here that this variant is accompanied with significant retention within the ER. Collectively, the retention of VWF in the ER, which would prevent it from progressing to WPBs from where it can be released via basal and stimulus-induced secretion, appears to be a common mechanism in VWD that could explain the lower circulating levels of VWF and the subsequent non-response to DDAVP.

In this study we show that circulating VWF plasma levels correlate with the amount of VWF contained in ECFCs and with the amount of VWF that is released from ECFCs upon stimulated secretion, which confirms the relevance of the ECFCs as *ex vivo* cell models for VWF secretion *in vivo*. Moreover, we show that protein levels of various secretion machinery proteins such as RAB27A, RAB3D, VWF and SYTL4 were significantly correlated to stimulated release of VWF and WPB count. Taken together this suggests that the exocytotic machinery that is recruited to WPBs is a determinant of circulating VWF, which is in line with previous findings from genome wide association studies that identified components of the secretory pathway such as *STX2* and *STXBP5* as determinants of VWF plasma levels (72-74). Interestingly, the correlation between plasma VWF:Ag and ECFC VWF levels (intracellular and released after stimulus) was only observed in cluster 1 cobblestone ECFCs, and not in cluster 2 mesenchymal/inflamed-like ECFCs. This raises the question whether cluster 2 ECFCs are representative of the endothelial compartment that is responsible for production of VWF that circulates in plasma and underscores the intricate connection between VWF and inflammation (75).

A limitation of this study was that patient characteristics were very diverse and despite ECFC matching, no common cause for the VWD phenotype was found. ECFC variation between groups was not representative of individual patient heterogeneity. Therefore, we focused on patient-specific qualitative findings rather than quantitative results. Our findings remain to be validated in a different setting or larger cohort to confirm whether these are patient-specific differences that contribute to the bleeding phenotype or arise from ECFC variation. Furthermore, other functional aspects like angiogenesis, proliferation and apoptosis were not included in this study. Analysis on ECFCs from patients with a bleeding disorder of unknown cause (BDUC), especially those with gastrointestinal bleeding might benefit from those assays. Moreover, as bleeding is mediated through the interplay of different cells, incorporation of multiple cell types such as platelets and leukocytes or the addition of shear stress in a flow model might boost future studies in unraveling VWD bleeding phenotypes.

Finally, to our knowledge this study is the first to examine a large panel of ECFCs of both healthy and VWD donors through extensive characterization by both functional assays and proteomics. As such, it highlights the current opportunities and challenges in using ECFCs as a model to study WPB-specific mechanisms and provides a broad EC-wide picture of the molecular regulation of WPB machinery and its outcomes.

Acknowledgements

The SYMPHONY consortium, which aims to orchestrate personalized treatment in patients with bleeding disorders, is a unique collaboration between patients, health care professionals, and translational and fundamental researchers specializing in inherited bleeding disorders, as well as experts from multiple disciplines (76). It aims to identify the best treatment choice for each individual based on bleeding phenotype. To achieve this goal, work packages (WP) have been organized according to 3 themes (e.g. Diagnostics [WPs 3 and 4], Treatment [WPs 5-9], and Fundamental Research [WPs 10-12]). Principal investigator: M.H. Cnossen; project manager: S.H. Reitsma.

Beneficiaries of the SYMPHONY consortium: Erasmus University Medical Center-Sophia Children's Hospital, project leadership and coordination; Sanquin Diagnostics; Sanquin Research; Amsterdam University Medical Centers; University Medical Center Groningen; University Medical Center Utrecht; Leiden University Medical Center; Radboud University Medical Center; Netherlands Society of Hemophilia Patients (NVHP); Netherlands Society for Thrombosis and Hemostasis (NVTH); Bayer B.V., CSL Behring B.V., Swedish Orphan Biovitrum (Belgium) BVBA/SPRL.

Funding by SYMPHONY: NWO-NWA.1160.18.038 (received by SNJL, IvM, RB and JE), Landsteiner Foundation for Blood Transfusion Research, Grant Number:1707 (received by RB).

We would like to acknowledge Suzan de Boer, Yvonne Jongejan, Noa Linthorst, Isabel Bär, Sophie Hordijk, Calvin van Kwawegen and Ferdows Atiq for their collaboration and assistance with patient selection, inclusion and ECFC isolation and culture.

Authorship Contributions

SNJL, RJD, SG, PB performed research; SNJL, RJD, SG analyzed data; SNJL, RJD, IvM, SG, MvB, FL, PB, RB and JE designed the research and wrote the paper and provided feedback on the manuscript.

Conflicts of interest

The WiN study was supported by the Dutch Haemophilia Foundation, the Erasmus MC, CSL Behring and Takeda (funding obtained by FL). FL is a consultant for CSL Behring, Biomarin, and Takeda of which the fees go to the university. JE received research funding from CSL Behring which funds go to the university.

All other authors declare no conflicts of interest.

Data availability

All data files are available in a repository; https://figshare.com/projects/Data_repository_-_Von_Willebrand_disease-specific_defects_and_proteomic_signatures_in_endothelial_colony_forming_cells/229449

Proteome raw- and search-files have been deposited in the ProteomeXchange Consortium (<http://proteomecentral.proteomexchange.org/cgi/GetDataset>) via the PRIDE partner repository with the dataset identifier *PXD055124*.

References

1. Valentijn KM, Sadler JE, Valentijn JA, Voorberg J, Eikenboom J. Functional architecture of Weibel-Palade bodies. *Blood*. 2011;117(19):5033-43.
2. Hordijk S, Carter T, Bierings R. A new look at an old body: molecular determinants of Weibel-Palade body composition and von Willebrand factor exocytosis. *J Thromb Haemost*. 2024;22(5):1290-303.
3. Schillemans M, Karampini E, Kat M, Bierings R. Exocytosis of Weibel-Palade bodies: how to unpack a vascular emergency kit. *J Thromb Haemost*. 2019;17(1):6-18.
4. Leebeek FWG, Eikenboom JCJ. Von Willebrand's Disease. *New England Journal of Medicine*. 2016;375(21):2067-80.
5. Murray EW, Lillcrap D. von Willebrand disease: pathogenesis, classification, and management. *Transfus Med Rev*. 1996;10(2):93-110.
6. Castaman G. How I treat von Willebrand disease. *Thromb Res*. 2020;196:618-25.
7. Atiq F, Heijdra J, Snijders F, Boender J, Kempers E, van Heerde WL, et al. Desmopressin response depends on the presence and type of genetic variants in patients with type 1 and type 2 von Willebrand disease. *Blood Adv*. 2022;6(18):5317-26.
8. Biguzzi E, Siboni SM, Peyvandi F. Acquired Von Willebrand syndrome and response to desmopressin. *Haemophilia*. 2018;24(1):e25-e8.
9. Castaman G, Lethagen S, Federici AB, Tosetto A, Goodeve A, Budde U, et al. Response to desmopressin is influenced by the genotype and phenotype in type 1 von Willebrand disease (VWD): results from the European Study MCMDM-1VWD. *Blood*. 2008;111(7):3531-9.
10. Castaman G, Mancuso ME, Giacomelli SH, Tosetto A, Santagostino E, Mannucci PM, et al. Molecular and phenotypic determinants of the response to desmopressin in adult patients with mild hemophilia A. *J Thromb Haemost*. 2009;7(11):1824-31.
11. Castaman G, Tosetto A, Eikenboom JC, Rodeghiero F. Blood group significantly influences von Willebrand factor increase and half-life after desmopressin in von Willebrand disease Vicenza. *J Thromb Haemost*. 2010;8(9):2078-80.
12. Castaman G, Rodeghiero F. No influence of blood group on the responsiveness to desmopressin in type I "platelet normal" von Willebrand's disease. *Thromb Haemost*. 1995;73(3):551-2.
13. Di Perna C, Riccardi F, Franchini M, Rivolta GF, Pattacini C, Tagliaferri A. Clinical efficacy and determinants of response to treatment with desmopressin in mild hemophilia a. *Semin Thromb Hemost*. 2013;39(7):732-9.
14. Lethagen S, Egervall K, Berntorp E, Bengtsson B. The administration of desmopressin by nasal spray: a dose-determination study in patients with mild haemophilia A or von Willebrand's disease. *Haemophilia*. 1995;1(2):97-102.
15. Nance D, Fletcher SN, Bolgiano DC, Thompson AR, Josephson NC, Konkle BA. Factor VIII mutation and desmopressin-responsiveness in 62 patients with mild haemophilia A. *Haemophilia*. 2013;19(5):720-6.
16. Revel-Vilk S, Schmutz M, Carcao MD, Blanchette P, Rand ML, Blanchette VS. Desmopressin (DDAVP) responsiveness in children with von Willebrand disease. *J Pediatr Hematol Oncol*. 2003;25(11):874-9.
17. Revel-Vilk S, Blanchette VS, Sparling C, Stain AM, Carcao MD. DDAVP challenge tests in boys with mild/moderate haemophilia A. *Br J Haematol*. 2002;117(4):947-51.

18. Seary ME, Feldman D, Carcao MD. DDAVP responsiveness in children with mild or moderate haemophilia A correlates with age, endogenous FVIII:C level and with haemophilic genotype. *Haemophilia*. 2012;18(1):50-5.
19. Sharthkumar A, Greist A, Di Paola J, Winay J, Roberson C, Heiman M, et al. Biologic response to subcutaneous and intranasal therapy with desmopressin in a large Amish kindred with Type 2M von Willebrand disease. *Haemophilia*. 2008;14(3):539-48.
20. Stoof SC, Sanders YV, Petrij F, Cnossen MH, de Maat MP, Leebeek FW, et al. Response to desmopressin is strongly dependent on F8 gene mutation type in mild and moderate haemophilia A. *Thromb Haemost*. 2013;109(3):440-9.
21. de Jong A, Eikenboom J. Von Willebrand disease mutation spectrum and associated mutation mechanisms. *Thromb Res*. 2017;159:65-75.
22. James PD, Notley C, Hegadorn C, Leggo J, Tuttle A, Tinlin S, et al. The mutational spectrum of type 1 von Willebrand disease: Results from a Canadian cohort study. *Blood*. 2007;109(1):145-54.
23. Lavin M, Aguila S, Schneppenheim S, Dalton N, Jones KL, O'Sullivan JM, et al. Novel insights into the clinical phenotype and pathophysiology underlying low VWF levels. *Blood*. 2017;130(21):2344-53.
24. Atiq F, Boender J, van Heerde WL, Tellez Garcia JM, Schoormans SC, Krouwel S, et al. Importance of Genotyping in von Willebrand Disease to Elucidate Pathogenic Mechanisms and Variability in Phenotype. *Hemasphere*. 2022;6(6):e718.
25. Swystun LL, Lillicrap D. Genetic regulation of plasma von Willebrand factor levels in health and disease. *J Thromb Haemost*. 2018;16(12):2375-90.
26. de Boer S, Eikenboom J. Von Willebrand Disease: From In Vivo to In Vitro Disease Models. *Hemasphere*. 2019;3(5):e297.
27. Wang JW, Bouwens EA, Pintao MC, Voorberg J, Safdar H, Valentijn KM, et al. Analysis of the storage and secretion of von Willebrand factor in blood outgrowth endothelial cells derived from patients with von Willebrand disease. *Blood*. 2013;121(14):2762-72.
28. Selvam SN, Casey LJ, Bowman ML, Hawke LG, Longmore AJ, Mewburn J, et al. Abnormal angiogenesis in blood outgrowth endothelial cells derived from von Willebrand disease patients. *Blood Coagul Fibrinolysis*. 2017;28(7):521-33.
29. Starke RD, Paschalaki KE, Dyer CE, Harrison-Lavoie KJ, Cutler JA, McKinnon TA, et al. Cellular and molecular basis of von Willebrand disease: studies on blood outgrowth endothelial cells. *Blood*. 2013;121(14):2773-84.
30. Laan SNJ, Lenderink BG, Eikenboom JCJ, Bierings R. Endothelial colony-forming cells in the spotlight: insights into the pathophysiology of von Willebrand disease and rare bleeding disorders. *Journal of Thrombosis and Haemostasis*. 2024;22(12):3355-65.
31. Bar I, Barraclough A, Burgisser PE, van Kwawegen C, Fijnvandraat K, Eikenboom JCJ, et al. The severe von Willebrand disease variant p.M771V leads to impaired anterograde trafficking of von Willebrand factor in patient-derived and base-edited endothelial colony-forming cells. *J Thromb Haemost*. 2024.
32. de Wee EM, Sanders YV, Mauser-Bunschoten EP, van der Bom JG, Degenaar-Dujardin ME, Eikenboom J, et al. Determinants of bleeding phenotype in adult patients with moderate or severe von Willebrand disease. *Thromb Haemost*. 2012;108(4):683-92.
33. Rodeghiero F, Tosetto A, Abshire T, Arnold DM, Collier B, James P, et al. ISTH/SSC bleeding assessment tool: a standardized questionnaire and a proposal for a new bleeding score for inherited bleeding disorders. *J Thromb Haemost*. 2010;8(9):2063-5.

34. de Boer S, Bowman M, Notley C, Mo A, Lima P, de Jong A, et al. Endothelial characteristics in healthy endothelial colony forming cells; generating a robust and valid ex vivo model for vascular disease. *J Thromb Haemost.* 2020;18(10):2721-31.
35. Laan SNJ, de Boer S, Dirven RJ, van Moort I, Kuipers TB, Mei H, et al. Transcriptional and functional profiling identifies inflammation and endothelial-to-mesenchymal transition as potential drivers for phenotypic heterogeneity within a cohort of endothelial colony forming cells. *J Thromb Haemost.* 2024;22(7):2027-38.
36. Stirling DR, Swain-Bowden MJ, Lucas AM, Carpenter AE, Cimini BA, Goodman A. CellProfiler 4: improvements in speed, utility and usability. *BMC Bioinformatics.* 2021;22(1):433.
37. Laan SNJ, Dirven RJ, Bürgisser PE, Eikenboom J, Bierings R. Automated segmentation and quantitative analysis of organelle morphology, localization and content using CellProfiler. *PLoS One.* 2023;18(6):e0278009.
38. de Jong A, Weijers E, Dirven R, de Boer S, Streur J, Eikenboom J. Variability of von Willebrand factor-related parameters in endothelial colony forming cells. *J Thromb Haemost.* 2019;17(9):1544-54.
39. Groten SA, Smit ER, van den Biggelaar M, Hoogendijk AJ. The proteomic landscape of in vitro cultured endothelial cells across vascular beds. *Commun Biol.* 2024;7(1):989.
40. Skowronek P, Thielert M, Voytik E, Tanzer MC, Hansen FM, Willems S, et al. Rapid and In-Depth Coverage of the (Phospho-)Proteome With Deep Libraries and Optimal Window Design for dia-PASEF. *Molecular & Cellular Proteomics.* 2022;21(9):100279.
41. Martin Maechler PR, Anja Struyf, Mia Hubert, Kurt Hornik. cluster: Cluster Analysis Basics and Extensions 2023 [Available from: <https://CRAN.R-project.org/package=cluster>].
42. Ritchie ME, Phipson B, Wu D, Hu Y, Law CW, Shi W, et al. limma powers differential expression analyses for RNA-sequencing and microarray studies. *Nucleic Acids Res.* 2015;43(7):e47.
43. Phipson B, Lee S, Majewski JJ, Alexander WS, Smyth GK. Robust Hyperparameter Estimation Protects against Hypervariable Genes and Improves Power to Detect Differential Expression. *Ann Appl Stat.* 2016;10(2):946-63.
44. F HJ. Hmisc: Harrell Miscellaneous. R package version 5.1-4. 2024.
45. Yu G, Wang LG, Han Y, He QY. clusterProfiler: an R package for comparing biological themes among gene clusters. *Omic.* 2012;16(5):284-7.
46. James PD, Connell NT, Ameer B, Di Paola J, Eikenboom J, Giraud N, et al. ASH ISTH NHF WFH 2021 guidelines on the diagnosis of von Willebrand disease. *Blood Adv.* 2021;5(1):280-300.
47. Sanders YV, Giezenaar MA, Laros-van Gorkom BA, Meijer K, van der Bom JG, Cnossen MH, et al. von Willebrand disease and aging: an evolving phenotype. *J Thromb Haemost.* 2014;12(7):1066-75.
48. Rydz N, Grabell J, Lillicrap D, James PD. Changes in von Willebrand factor level and von Willebrand activity with age in type 1 von Willebrand disease. *Haemophilia.* 2015;21(5):636-41.
49. Atiq F, Blok R, van Kwawegen CB, Doherty D, Lavin M, van der Bom JG, et al. Type 1 VWD classification revisited: novel insights from combined analysis of the LoVIC and WiN studies. *Blood.* 2024;143(14):1414-24.
50. Starke RD, Ferraro F, Paschalaki KE, Dryden NH, McKinnon TA, Sutton RE, et al. Endothelial von Willebrand factor regulates angiogenesis. *Blood.* 2011;117(3):1071-80.
51. Groeneveld DJ, van Bekkum T, Dirven RJ, Wang JW, Voorberg J, Reitsma PH, et al. Angiogenic characteristics of blood outgrowth endothelial cells from patients with von Willebrand disease. *J Thromb Haemost.* 2015;13(10):1854-66.

52. Dai Y, Hu R, Liu A, Cho KS, Manuel AM, Li X, et al. WebCSEA: web-based cell-type-specific enrichment analysis of genes. *Nucleic Acids Research*. 2022;50(W1):W782-W90.
53. Harvey NL, Srinivasan RS, Dillard ME, Johnson NC, Witte MH, Boyd K, et al. Lymphatic vascular defects promoted by Prox1 haploinsufficiency cause adult-onset obesity. *Nature Genetics*. 2005;37(10):1072-81.
54. Wigle JT, Oliver G. Prox1 function is required for the development of the murine lymphatic system. *Cell*. 1999;98(6):769-78.
55. Chen JM, Luo B, Ma R, Luo XX, Chen YS, Li Y. Lymphatic Endothelial Markers and Tumor Lymphangiogenesis Assessment in Human Breast Cancer. *Diagnostics (Basel)*. 2021;12(1).
56. Zografou S, Basagiannis D, Papafotika A, Shirakawa R, Horiuchi H, Auerbach D, et al. A complete Rab screening reveals novel insights in Weibel-Palade body exocytosis. *J Cell Sci*. 2012;125(Pt 20):4780-90.
57. Bierings R, Hellen N, Kiskin N, Knipe L, Fonseca AV, Patel B, et al. The interplay between the Rab27A effectors Slp4-a and MyRIP controls hormone-evoked Weibel-Palade body exocytosis. *Blood*. 2012;120(13):2757-67.
58. Knop M, Aaeskjold E, Bode G, Gerke V. Rab3D and annexin A2 play a role in regulated secretion of vWF, but not tPA, from endothelial cells. *Embo j*. 2004;23(15):2982-92.
59. van Breevoort D, van Agtmaal EL, Dragt BS, Gebbink JK, Dienava-Verdoold I, Kragt A, et al. Proteomic Screen Identifies IGFBP7 as a Novel Component of Endothelial Cell-Specific Weibel-Palade Bodies. *Journal of Proteome Research*. 2012;11(5):2925-36.
60. Yamazaki Y, Eura Y, Kokame K. V-ATPase V0a1 promotes Weibel-Palade body biogenesis through the regulation of membrane fission. *Elife*. 2021;10.
61. Terglane J, Menche D, Gerke V. Acidification of endothelial Weibel-Palade bodies is mediated by the vacuolar-type H⁺-ATPase. *PLoS One*. 2022;17(6):e0270299.
62. Medina RJ, O'Neill CL, O'Doherty TM, Chambers SE, Guduric-Fuchs J, Neisen J, et al. Ex vivo expansion of human outgrowth endothelial cells leads to IL-8-mediated replicative senescence and impaired vasoreparative function. *Stem Cells*. 2013;31(8):1657-68.
63. Smadja DM, Bièche I, Uzan G, Bompais H, Muller L, Boisson-Vidal C, et al. PAR-1 activation on human late endothelial progenitor cells enhances angiogenesis in vitro with upregulation of the SDF-1/CXCR4 system. *Arterioscler Thromb Vasc Biol*. 2005;25(11):2321-7.
64. Bompais H, Chagraoui J, Canron X, Crisan M, Liu XH, Anjo A, et al. Human endothelial cells derived from circulating progenitors display specific functional properties compared with mature vessel wall endothelial cells. *Blood*. 2004;103(7):2577-84.
65. Dejana E, Hirschi KK, Simons M. The molecular basis of endothelial cell plasticity. *Nature Communications*. 2017;8(1):14361.
66. Potente M, Mäkinen T. Vascular heterogeneity and specialization in development and disease. *Nature Reviews Molecular Cell Biology*. 2017;18(8):477-94.
67. Wigle JT, Harvey N, Detmar M, Lagutina I, Grosveld G, Gunn MD, et al. An essential role for Prox1 in the induction of the lymphatic endothelial cell phenotype. *Embo j*. 2002;21(7):1505-13.
68. Kilic N, Oliveira-Ferrer L, Neshat-Vahid S, Irmak S, Obst-Pernberg K, Wurmbach J-H, et al. Lymphatic reprogramming of microvascular endothelial cells by CEA-related cell adhesion molecule-1 via interaction with VEGFR-3 and Prox1. *Blood*. 2007;110(13):4223-33.

69. HICKSON N, HAMPSHIRE D, WINSHIP P, GOUDEMAMAND J, SCHNEPPENHEIM R, BUDDE U, et al. von Willebrand factor variant p.Arg924Gln marks an allele associated with reduced von Willebrand factor and factor VIII levels. *Journal of Thrombosis and Haemostasis*. 2010;8(9):1986-93.
70. Yin J, Ma Z, Su J, Wang J-W, Zhao X, Ling J, et al. Mutations in the D1 domain of von Willebrand factor impair their propeptide-dependent multimerization, intracellular trafficking and secretion. *Journal of Hematology & Oncology*. 2015;8(1):73.
71. Penas N, Pérez-Rodríguez A, Torea JH, Lourés E, Noya MS, López-Fernández MF, et al. von Willebrand disease R1374C: type 2A or 2M? A challenge to the revised classification. High frequency in the northwest of Spain (Galicia). *Am J Hematol*. 2005;80(3):188-96.
72. Smith NL, Chen MH, Dehghan A, Strachan DP, Basu S, Soranzo N, et al. Novel associations of multiple genetic loci with plasma levels of factor VII, factor VIII, and von Willebrand factor: The CHARGE (Cohorts for Heart and Aging Research in Genome Epidemiology) Consortium. *Circulation*. 2010;121(12):1382-92.
73. Sanders YV, van der Bom JG, Isaacs A, Cnossen MH, de Maat MP, Laros-van Gorkom BA, et al. CLEC4M and STXBP5 gene variations contribute to von Willebrand factor level variation in von Willebrand disease. *J Thromb Haemost*. 2015;13(6):956-66.
74. van Loon JE, Leebeek FW, Deckers JW, Dippel DW, Poldermans D, Strachan DP, et al. Effect of genetic variations in syntaxin-binding protein-5 and syntaxin-2 on von Willebrand factor concentration and cardiovascular risk. *Circ Cardiovasc Genet*. 2010;3(6):507-12.
75. Drakeford C, Aguila S, Roche F, Hokamp K, Fazavana J, Cervantes MP, et al. von Willebrand factor links primary hemostasis to innate immunity. *Nature Communications*. 2022;13(1):6320.
76. Cnossen MH, van Moort I, Reitsma SH, de Maat MPM, Schutgens REG, Urbanus RT, et al. SYMPHONY consortium: Orchestrating personalized treatment for patients with bleeding disorders. *J Thromb Haemost*. 2022;20(9):2001-11.

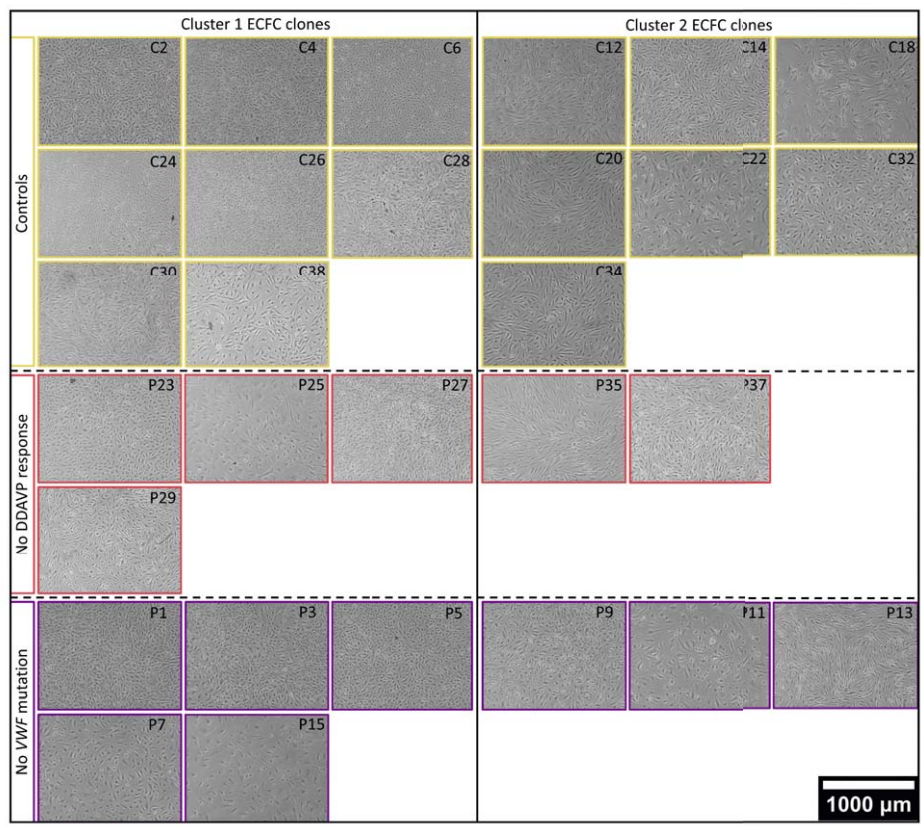
Supplemental table 1. Antibodies used in immunofluorescence

Antibody	Manufacturer	Category number	Concentration	Dilution
IF Primary antibodies				
VWF (Rabbit)	DAKO	A0082	4.1 mg/mL	1:1,000
VE-cadherin (Mouse)	BD Pharming	555661	0.5 mg/mL	1:250
VWF (Sheep)	Abcam	AB11743	1 mg/mL	1:1,000
PDI (Rabbit)	Enzo life sciences	SPA-890	1 mg/mL	1:250
Hoechst	Thermo Fisher Scientific	H3569	10 mg/mL	1:10,000
IF Secondary antibodies				
Donkey-anti-Sheep AF488	Invitrogen Molecular Probes	A11015	2 mg/mL	1:750
Donkey-anti-Mouse AF488	Invitrogen Molecular Probes	A21202	2 mg/mL	1:750
Donkey-anti-Mouse AF568	Invitrogen Molecular Probes	A10037	2 mg/mL	1:750
Donkey-anti-Rabbit AF647	Invitrogen Molecular Probes	A31573	2 mg/mL	1:750

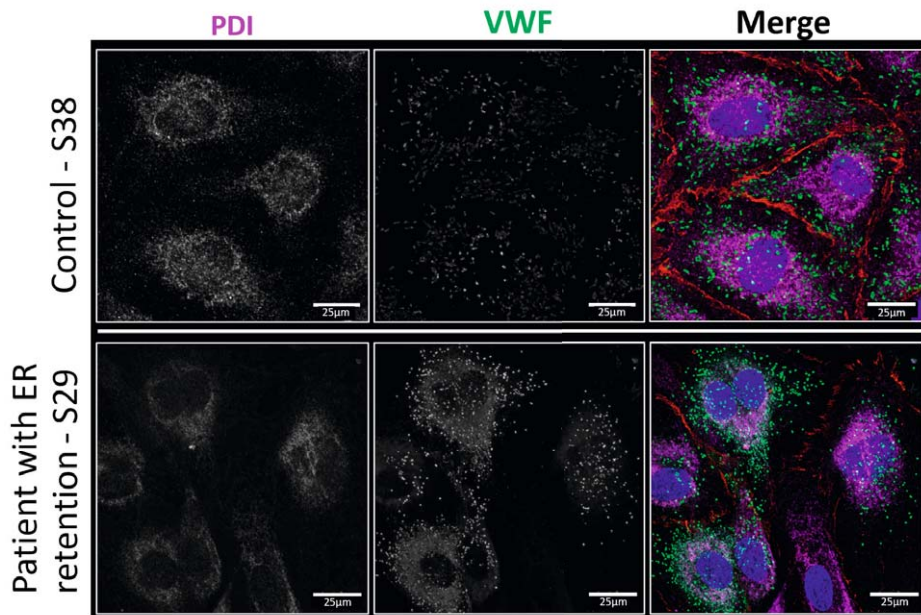
Abbreviations: Von Willebrand Factor (VWF), Immunofluorescence (IF)

Supplemental table 2. Primer sequences used for the qPCR panel

Gene	Sense	Anti-sense
GAPDH	ACCATCTTCCAGGAGCGAGA	GACTCCACGACGTACTCAGC
RAB27A	GAAGCCATAGCACTCGCAGAGA	CAGGACTTGTCCACACACCGTT
SELP	TCCGCTGCATTGACTCTGGACA	CTGAAACGCTCTCAAGGATGGAG
VWF	TTGACGGGGAGGTGAATGTG	ATGTCTGCTTCAGGACCACG
PLAT	TGGTGCTACGTCTTTAAGGCGG	GCTGACCCATTCCTCAAAGTAGC
CD63	CAACCACACTGCTTCGATCCTG	GACTCGGTTCTTCGACATGGAAG
ALDH1A1	CGGGAAAAGCAATCTGAAGAGGG	GATGCGGCTATACAACACTGGC
SOX18	GTGTGGGCAAAGGACGAG	GTTCAGCTCCTTCCACGCT
BMP2	TGTATCGCAGGCACTCAGGTCA	CCACTCGTTTCTGGTAGTTCTTC
COL1A1	CAGCCGCTTCACCTACAGC	TTTTGTATTCAATCACTGTCTTGCC
TGFB β	GGACATGCTCACTATCAACGGG	CTGTGGACACATCAGACTCTGC
IFI27	CGTCCTCCATAGCAGCCAAGAT	ACCCAATGGAGCCCAGGATGAA
BST2	TCTCCTGCAACAAGAGCTGACC	TCTCTGCATCCAGGGAAGCCAT
ABI3BP	CCTTCTACACCTAAACGACGCC	GGTGTTGTCCATGTAGGTTTCAGG
SERPINE1	CTCATCAGCCACTGGAAAGGCA	GACTCGTGAAGTCAGCCTGAAAC
CXCL8	GAGAGTGATTGAGAGTGGACCAC	CACAACCCTCTGCACCCAGTTT



Supplemental Figure 1. Brightfield images of all isolated ECFC clones. Images taken by brightfield microscopy with a 5x magnification. Scale is 1,000 μm. Image border indicates to which group the clone belongs, control (yellow), VWD patients without DDAVP response (red) and VWD patients without VWF variant (purple). Abbreviations: VWF = von Willebrand factor; ECFC = Endothelial colony forming cell; DDAVP = 1-deamino-8-D-arginine vasopressin.

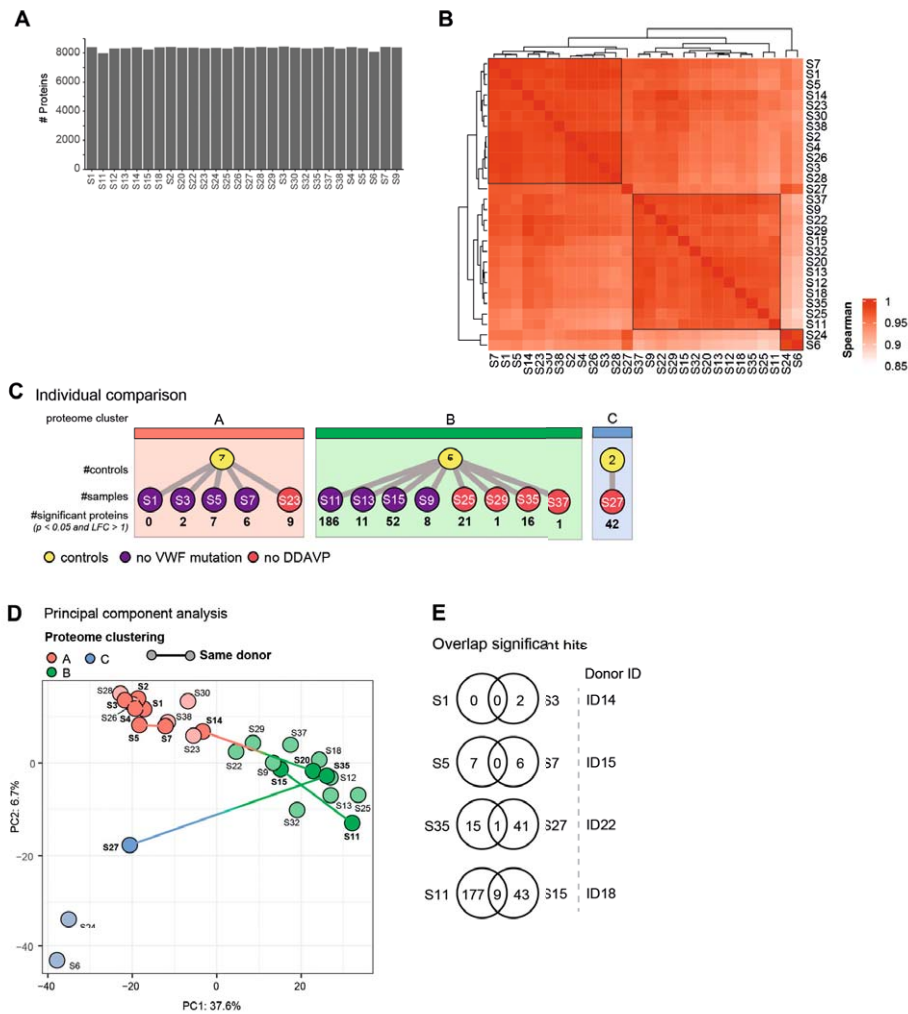


Supplemental Figure 2. Retention of VWF in the ER in representative image. Detailed imaging of ECFCs was done using airyscan super resolution confocal microscopy with a 63x objective. ECFC clones were imaged during the isolation process just before freezing. Representative confocal images of a control ECFC clone (top - S38) and patient ECFCs with retention of VWF in the ER (bottom - S29) stained with Hoechst (blue) and antibodies against VE-cadherin (red), PDI to stain the ER (Magenta) and VWF (green). Scale bar represents 25 µm. In white, the overlap between the VWF and PDI signal is shown. Abbreviations: VWF = von Willebrand factor; PDI = protein disulfide isomerase; ER = endoplasmic reticulum.

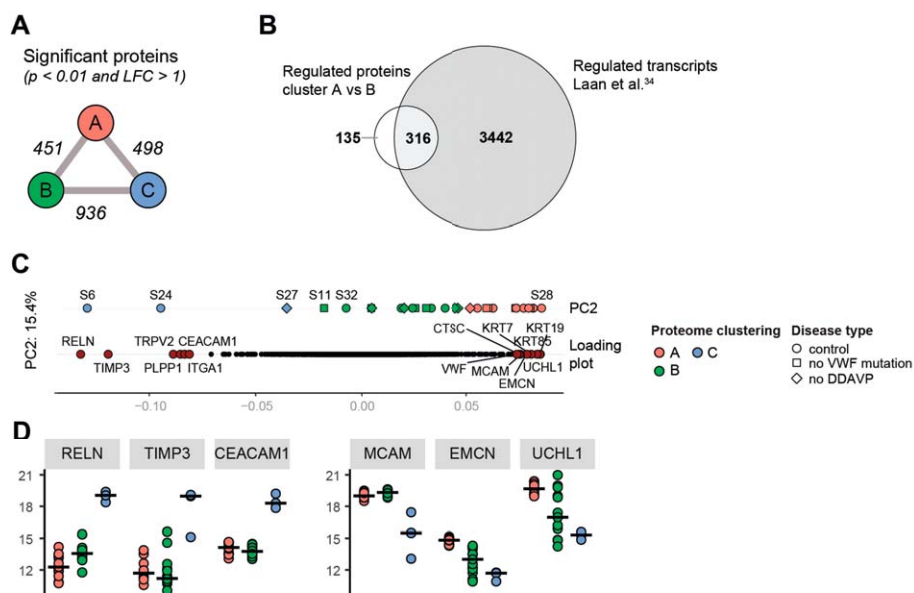


7

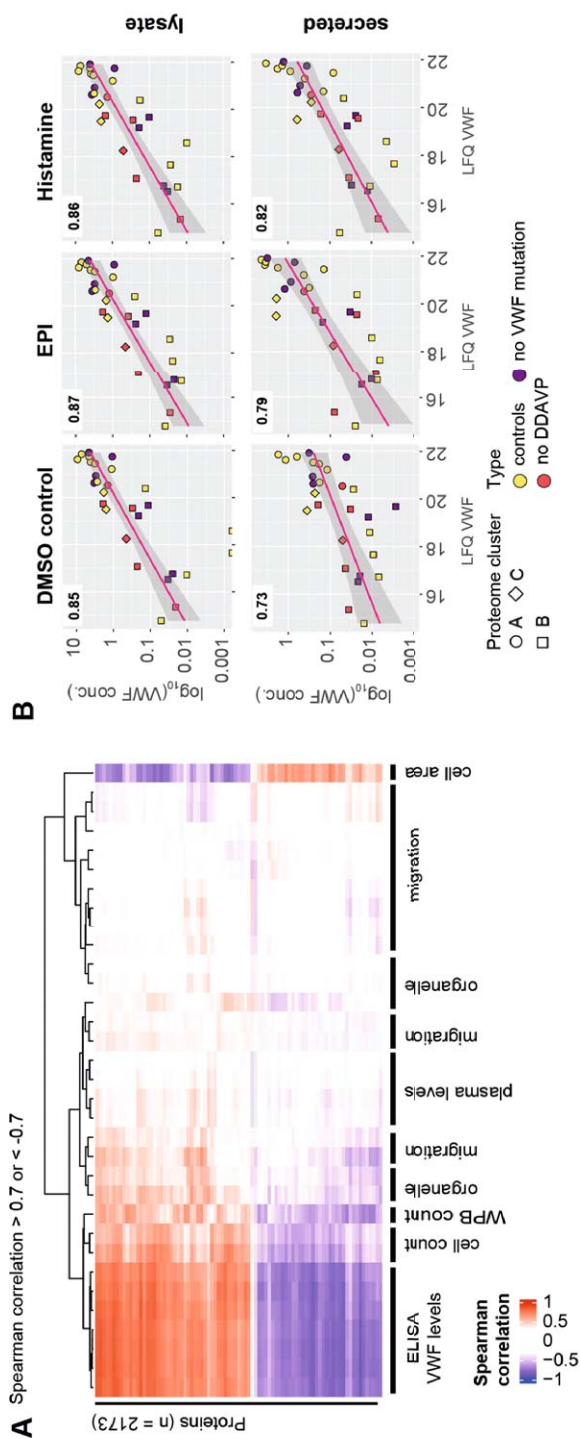
t=0 was added as a single data point. Time points 1, 2 and 3 had to be removed due to shifting of the plate during image acquisition. C) Average maximum speed per clone (left), X trajectory (middle) and linearity calculated as displacement / integrated distance (right) for cluster 1 and cluster 2 ECFCs. Statistical analysis by Kruskal-Wallis one way ANOVA, * p < 0.05. Abbreviations: DDAVP = 1-deamino-8-D-arginine vasopressin; VWF = von Willebrand factor; ns = not significant.



Supplemental Figure 4 A) Bar graph showing number of quantified proteins per sample. B) Heatmap of spearman correlation between samples, three groups are indicated by black squares. Overview of samples and significantly regulated proteins (t-test, p < 0.05 and LFC > 1) between C) individual patient ECFC clones versus controls per proteome cluster. D) Principal component analysis (PCA) of proteomes across PC1 and PC2, samples are labeled, clones from the same donor are connected, colors indicate proteome cluster (Cluster A - green, Cluster B - red, Cluster C - blue). E) Overlap in significant hits of ECFCs clones derived from the same donor.



Supplemental Figure 5 A) Number of significant hits (t-test, p value < 0.05 , $LFC > 1$) between proteome clusters as indicated. B) Overlap of significantly regulated proteins between cluster A and B versus regulated transcripts in Laan *et al.* (35) C) Distribution of samples and loading plot across PC2, shape indicates disease type (control – circle, no DDAVP – diamond, no VWF mutation – square). Highest positive and negative separating proteins in the loading plot are highlighted in red and labeled. D) Dot plots of protein LFQ values with high positive and negative separation across PC2.



Supplemental Figure 6 A) Heatmap showing protein Spearman correlation > 0.7 between LFQ-levels and functional assay output. Gradient indicates correlation. Functional output terms have been summarized. B) Correlation plots of LFQ levels and ELISA VWF levels in lysates and secreted. Color indicates disease type: controls (yellow), no DDAVP (red) and no VWF mutation (purple), shapes indicate protein cluster: A (circle), B (square) and C (diamond).

Supplementary Methods

Plasma coagulation factor level measurements

VWF:Ag was measured using Polyclonal Rabbit Anti-Human Von Willebrand factor (Agilent Technologies) as coating antibody. Polyclonal Rabbit Anti-Human Von Willebrand factor Horseradish Peroxidase conjugated (Zebra Bioscience (Dako)), was used as detection antibody. 2,2'-azino-di-(3-ethylbenzthiazoline sulfonic acid) (ABTS) with 0.1% H_2O_2 was used as substrate buffer and the reaction was stopped by adding 5% acetic acid. Measurement was performed using the Synergy HT gen5™ microplate reader (Biotek). VWF:CB was measured using the HemosIL™ AcuStar system (kit 009802044) as per the manufacturer's protocol. VWF:Act was analyzed with a direct GPIb binding assay (VWF:GPIbM) using the INNOVANCE® VWF Ac (Siemens) as per manufacturer's protocol and measured using the sysmex CN3000 (Siemens). Finally, FVIII coagulation activity was measured by the automated one stage assay on the Sysmex CN3000 with FVIII deficient plasma (Siemens). Commercial pooled plasma (VisuA en VisuN (Stago)) was used as reference.

Automated quantification of ECFC migration

CellTracker Green signal was used to identify and count individual cells per time point in the migration assay. The area that was covered by cells was identified as the total area with cells, while the remaining area was identified as scratch. These parameters were used to calculate the cell density and the closing speed of the scratch. The timepoint where the scratch was closed was defined as the time of closure (ToC). In this study, the pipeline was expanded to include single cell measurements. The TrackObjects module was applied to recognize cell objects over time with a 50 pixel overlap. Objects were filtered out if they were measured in less than 20 frames. Of the tracked objects the displacement, integrated distance, linearity (calculated as displacement / integrated distance), distance traveled (speed), and X and Y trajectory were measured. For displacement, integrated distance and linearity the value at ToC was exported. For distance traveled, the max speed until ToC was exported. Finally, for X and Y trajectory, the average was taken until ToC.